Article

Cell Reports

Cholinergic control of striatal GABAergic microcircuits

Graphical abstract

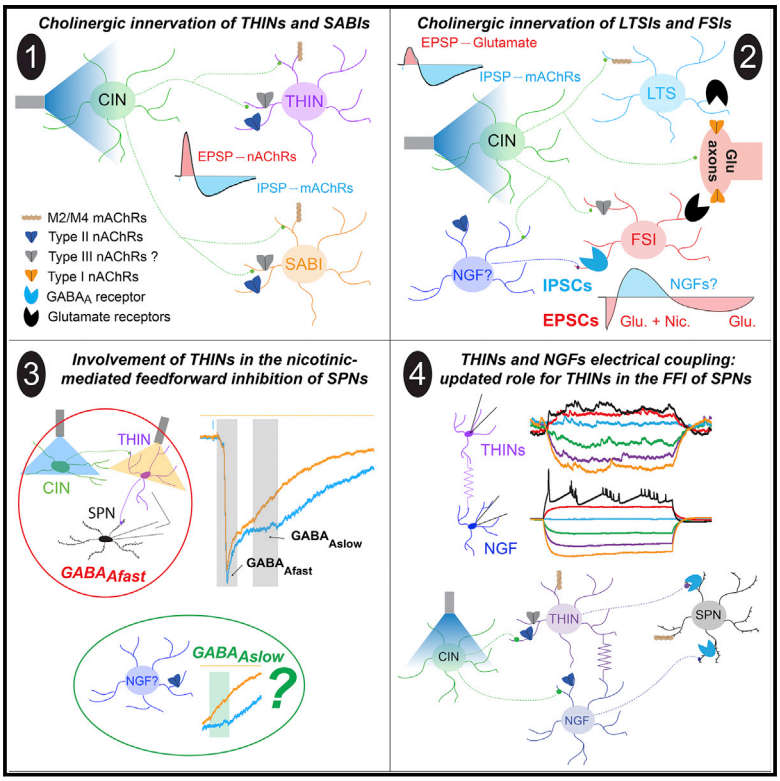

Highlights

- CINs innervate at least four populations of striatal GINs
- Mechanisms of innervation are complex involving nAChRs, mAChRs, glutamate, and GABA
- THINs participate in the CIN-mediated disynaptic feedforward inhibition of SPNs
- This principally involves heterotypic electrical coupling between THINs and NGFs

Authors

Samet Kocaturk, Elif Beyza Guven, Fulva Shah, James M. Tepper, Maxime Assous

Correspondence

assous.maxime@gmail.com

In brief

Kocaturk et al. show that cholinergic interneurons (CINs) innervate diverse populations of GABAergic interneurons (GINs). CIN stimulation triggers multiphasic responses in GINs involving synaptic and heterosynaptic mechanisms. Further, tyrosine hydroxylase-expressing interneurons (THINs) participate in the CIN-mediated disynaptic inhibition of SPNs via heterotypic electrical coupling with neurogliaform interneurons.

Kocaturk et al., 2022, Cell Reports *41*, 111531
October 25, 2022
https://doi.org/10.1016/j.celrep.2022.111531

CellPress

Cell Reports

CellPress
OPEN ACCESS

Article

Cholinergic control of striatal GABAergic microcircuits

Samet Kocaturk,[1] Elif Beyza Guven,[1] Fulva Shah,[1] James M. Tepper,[1] and Maxime Assous[1,2,*]
[1]Center for Molecular and Behavioral Neuroscience, Rutgers, the State University of New Jersey, 197 University Avenue, Newark, NJ 07102, USA
[2]Lead contact
*Correspondence: assous.maxime@gmail.com
https://doi.org/10.1016/j.celrep.2022.111531

SUMMARY

Cholinergic interneurons (CINs) are essential elements of striatal circuits and functions. Although acetylcholine signaling via muscarinic receptors (mAChRs) has been well studied, more recent data indicate that postsynaptic nicotinic receptors (nAChRs) located on striatal GABAergic interneurons (GINs) are equally critical. One example is that CIN stimulation induces large disynaptic inhibition of striatal projection neurons (SPNs) mediated by nAChR activation of GINs. Although these circuits are ideally positioned to modulate striatal output, the neurons involved are not definitively identified because of an incomplete mapping of CINs-GINs interconnections. Here, we show that CINs modulate four GINs populations via an intricate mechanism involving co-activation of presynaptic and postsynaptic mAChRs and nAChRs. Using optogenetics, we demonstrate the participation of tyrosine hydroxylase-expressing GINs in the disynaptic inhibition of SPNs via heterotypic electrical coupling with neurogliaform interneurons. Altogether, our results highlight the importance of CINs in regulating GINs microcircuits via complex synaptic/heterosynaptic mechanisms.

INTRODUCTION

The striatum possesses the highest density of acetylcholine (ACh) in the basal ganglia (BG, Mesulam et al., 1984), underlying the importance of ACh signaling in this structure. Striatal cholinergic interneurons (CINs) are responsible for the bulk of striatal ACh (Zhou et al., 2002).

Striatal muscarinic receptors (mAChRs) signaling has received particular attention because of their wide cellular distribution because they are expressed on the axon terminals of most striatal afferents, as well as by all striatal neurons examined, including the striatal projection neurons (SPNs; for review, see Assous, 2021; Goldberg et al., 2012). However, the functional role of mAChRs expressed by striatal GABAergic interneurons (GINs) is less known, with only a few electrophysiological studies (Elghaba et al., 2016; Koos and Tepper, 2002; Melendez-Zaidi et al., 2019).

The main role of nicotinic receptors (nAChRs) in the central nervous system has been suggested to be via the modulation of neurotransmitters release by presynaptic receptors (Dajas-Bailador and Wonnacott, 2004; Dani, 2001; Dani and Bertrand, 2007). Perhaps the most studied role of striatal nAChRs in this regard involves their expression on presynaptic dopaminergic and glutamatergic afferents, where they modulate the release of dopamine and glutamate (Rice and Cragg, 2004; Zhang and Sulzer, 2004; Zhou et al., 2001). However, we now know that CINs can also exert fast synaptic effects by activating subpopulations of striatal GINs via postsynaptic nAChRs, as has been observed in other brain structures, including the cortex and hippocampus (Assous, 2021; Bell et al., 2011; Dannenberg et al., 2017).

Indeed, stimulation of striatal cholinergic fibers evokes polysynaptic $GABA_A$ inhibitory post synaptic potentials / currents (IPSP/Cs) in CINs mediated by activation of type II, β2 subunit-containing nAChRs (β2-nAChRs), presumably expressed by striatal GINs (Dorst et al., 2020; Sullivan et al., 2008). Further, earlier indirect evidence demonstrated that nAChRs activation facilitates GABA-mediated inhibition of SPNs (de Rover et al., 2002; Koos and Tepper, 2002), and blockade of α4β2 nAChRs shortened SPN spike latencies following activation of corticostriatal projections (Matityahu et al., 2022).

We have previously demonstrated that optogenetic activation of CINs elicits large disynaptic GABAergic IPSP/Cs in SPNs that are secondary to β2-nAChR activation (English et al., 2012; Faust et al., 2016; Nelson et al., 2014b; Witten et al., 2010). The optically elicited IPSCs are kinetically biphasic consisting of a fast and a slow component, respectively, involving $GABA_{Afast}$- and $GABA_{Aslow}$-mediated currents (English et al., 2012). Although this nicotinic-mediated circuit is positioned to play a central role in the regulation of striatal neuronal activity and related functions, its neuronal composition is still mostly unknown. Although the $GABA_{Aslow}$ seems to rely on nicotinic activation of neurogliaform interneurons (NGFs) (English et al., 2012; Faust et al., 2016), the source(s) of the $GABA_{Afast}$ is still unclear but seems to involve multiple GINs targeted in the Htr3a-Cre mice (Faust et al., 2016).

Here, we performed a comprehensive analysis of the interconnections between CINs and various populations of GINs. By combining excitatory and inhibitory opsins, we dissected the participation of distinct populations of GINs in the disynaptic inhibition of SPNs. Our results demonstrate a heretofore unknown

organizational complexity of the CINs-GINs circuits, which play an important role in the regulation of striatal output activity. This study also underscores the relevance of relatively understudied postsynaptic nAChRs in the striatum and their potential implications for the development of targeted pharmacological approaches to treat associated disorders such as Parkinson's disease, dystonia, Tourette syndrome, or nicotine addiction.

RESULTS

CIN innervation of GINs

Our approach to identify the innervation of diverse populations of striatal GINs by CINs was to generate double-transgenic mice in which CINs (targeted via the expression of choline acetyltransferase, ChAT) natively express channelrhodopsin (ChR2) (ChAT-ChR2-eYFP) crossed with various Cre-expressing lines targeting different populations of GINs. Using a similar approach, we have previously demonstrated the cholinergic innervation of NGFs and fast-adapting interneurons (FAIs) (English et al., 2012; Faust et al., 2015).

CIN innervation of tyrosine hydroxylase-expressing interneurons (THINs)

Pharmacological studies demonstrated that most THINs respond to ACh agonists with strong depolarizations and action potential (AP) firing because of activation of nAChRs (Ibañez-Sandoval et al., 2015; Luo et al., 2013a). Further, recent evidence demonstrates monosynaptic connectivity between CINs and THINs (Dorst et al., 2020).

Here, we used double-transgenic ChAT-ChR2-eYFP::TH-Cre mice and transduced THINs with a adeno-associated virus (AAV)-Flex-td-Tomato (N = 16 mice; Figures 1A–1C). Optogenetic activation of CINs evoked large excitatory postsynaptic potentials/currents (EPSP/Cs) in almost all recorded THINs (n = 27/28; EPSP: 11.10 ± 1.43 mV, EPSC Vh −70 mV: −42.64 ± 7.73 pA; Figures 1E and 1F) that were sufficient to trigger AP (n = 20/27; Figures 1D and 1E). In most THINs, the EPSP/C was followed by an IPSP/C exhibiting slower kinetics (n = 23/27; IPSP amplitude: −1.57 ± 0.27 mV, τ = 725.34 ± 158.3 ms; Figures 1F–1H) able to induce a pause in the firing of THINs (Figure 1D).

Bath application of dihydro-β-erythroidine (DhβE; 1 μM), an antagonist selective for β2-nAChRs mostly consisting of type II nAChRs (Albuquerque et al., 1995, 2009), significantly reduced the amplitude of the excitatory response in THINs (−4.82 ± 0.87 mV, [−37.81%] versus control; Figures 1E–1G) and prevented CIN-induced AP firing (Figure 1E). The remaining EPSP/C was not affected by methyllycaconitine (MLA; 500 nM), an antagonist selective for α7-containing nAChR antagonist (type I nAChRs) mostly localized in the striatum presynaptically on glutamate afferents (Campos et al., 2010; Kaiser and Wonnacott, 2000). However, mecamylamine (MEC; 5 μM), a less selective nAChR antagonist, almost completely abolished the rest of the EPSP/Cs (−5.76 ± 1.33 mV [−72.6%] versus DhβE; one-way ANOVA, F(1.354, 16.25) = 25.43; Tukey's multiple comparisons, control versus DhβE: p = 0.0006; DhβE versus MLA: p = 0.42; MLA versus MEC: p = 0.0046; n = 13; Figures 1E–1G), indicating a mixed type II and type III nAChRs composition on THINs (but see caveats discussed below).

Bath application of AMPA and NMDA receptor antagonists (10 μM CNQX and 10 μM APV, respectively) reduced slightly but significantly the amplitude of the cholinergic-mediated excitatory response. Subsequent application of MEC largely abolished the remaining EPSCs (one-way ANOVA, F(1.015, 6.088) = 16.4, p = 0.0064; Tukey's multiple comparisons, control versus CNQX/APV: −3.68 ± 0.67 pA [−10.56%], p = 0.0037; CNQX/APV versus MEC: −25.63 ± 6.81 pA [−82.2%], p = 0.021; n = 7; Figures S1A and S1B).

Next, we tested the involvement of mAChRs on the slow IPSP/Cs induced by the stimulation of CINs. Atropine (10 μM) almost completely abolished the CIN-induced IPSP/Cs in THINs (−2.22 ± 0.71 mV [−95.7%] versus control; p = 0.035, t = 3.12, two-tailed paired t test; n = 5; Figures 1H and 1I), demonstrating its muscarinic nature.

Surprisingly, we also found that atropine significantly reduced the size of nAChR-mediated EPSP/Cs in THINs (−11.3 ± 4.15 pA [−17.3%]; p = 0.02, t = 2.72, two-tailed paired t test; n = 12; Figure S1C). However, this reduction was not reproduced with the M1 mAChR antagonist, VU0255035 (p = 0.18, two-tailed paired t test; n = 11; Figure S1D), or scopolamine, which significantly increased the EPSP/Cs (+14.18 ± 7.64 pA [+24.5%]; p = 0.00033, two-tailed paired t test; n = 16; Figure S1E), consistent with the elimination of the mAChR-mediated IPSCs.

These results demonstrate that CINs innervate striatal THINs with an intricate dual effect involving a nAChR-mediated excitation and a muscarinic-mediated inhibition (Figure 1J).

CIN innervation of spontaneously active bursty interneurons (SABIs)

To examine the connectivity between CINs and SABIs, we used double-transgenic ChAT-ChR2-eYFP:Htr3a-Cre mice and transduced Htr3a interneurons with td-Tomato as described above (N = 28 mice; Figures 2A–2C and S1F). As we described (Assous et al., 2018; Faust et al., 2015, 2016), targeted GINs in the Htr3a-Cre mice include fast spiking interneurons (FSIs) and NGFs, as well as FAIs and SABIs (Table S1). Optogenetic activation of CINs evoked large EPSP/Cs in all recorded SABIs (n = 67, EPSP: 11.49 ± 0.85 mV, n = 57; EPSC @ Vh = −70 mV: −65.51 ± 6.34 pA, τ = 49.8 ± 16.7 ms, n = 48; Figures 2D–2I and S1G–S1I) that were sufficient to trigger AP firing and characteristic bursts in cell-attached recordings (Figure 2D). In most SABIs, the cholinergic-induced EPSP/C was followed by an IPSP/C presenting slower kinetics (n = 54/67, IPSP amplitude: −2.38 ± 0.27 mV, n = 41, τ = 412.8 ± 64.02 ms; IPSC amplitude: 7.88 ± 1.07 pA, n = 32, τ = 278.7 ± 31.8 ms; Figures 2F–2H and S1G–S1I).

Application of DhβE reduced the amplitude of the excitatory response (−1.64 ± 0.41 mV [−18.3%] versus control; Figures 2F and 2G). The remaining EPSP/C was not affected by MLA but was greatly reduced by MEC (−4.78 ± 0.46 mV [−69.4%] versus MLA; one-way ANOVA, F(1.558, 21.81) = 77.4; Tukey's multiple comparisons, control versus DhβE: p = 0.0067; DhβE versus MLA: p = 0.248; MLA versus MEC: $p = 3 \times 10^{-7}$; n = 15; Figure 2G), indicating a mixed type II and type III nAChR composition.

Then we tested the effect of glutamate receptor antagonists. Bath application of AMPA and NMDA receptor antagonists (10 μM CNQX and 10 μM APV, respectively) did not affect the

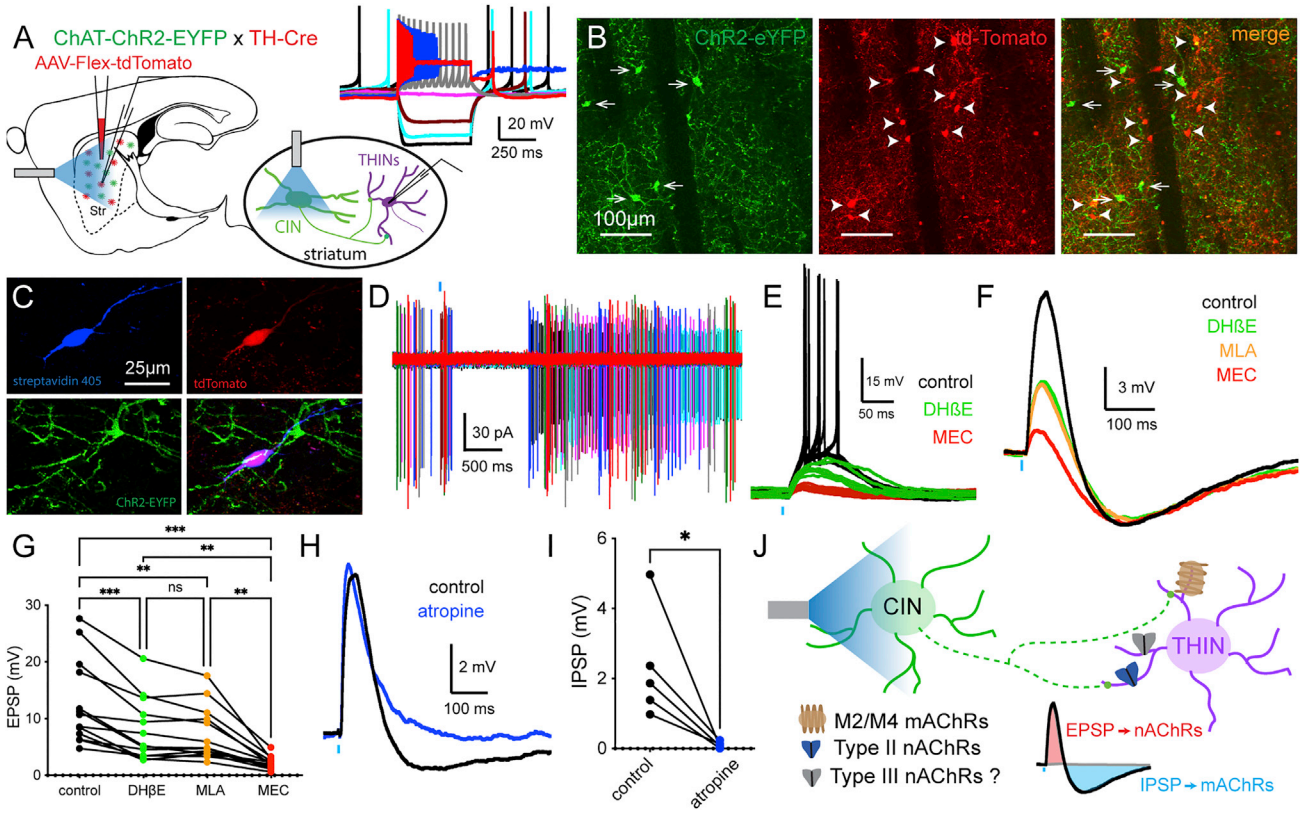

Figure 1. Cholinergic innervation of THINs

(A) Schematic illustrating the experimental design using double-transgenic ChAT-ChR2-eYFP:TH-Cre mice injected with a Cre-dependent td-Tomato AAV in the striatum. Inset: typical responses of a THIN to negative and positive somatic current injections.

(B) Confocal photomicrographs showing transduction of THINs (red) and CINs (green).

(C) Confocal photomicrographs of a recorded THIN, filled with biocytin (revealed with streptavidin 405, blue) and surrounded by ChR2 axons (green).

(D) Cell-attached recording of a THIN, which responds to optogenetic stimulation of CIN (blue bar) with a burst of APs.

(E) Current-clamp recording of a THIN firing APs in response to CIN stimulation (black traces). DhβE (1 μM, green traces) prevents CIN-induced AP firing leaving subthreshold EPSPs. MEC (5 μM, red traces) almost completely abolished the EPSP.

(F) Current-clamp recording of a THIN following CIN optogenetic stimulation (black trace is control), showing a large EPSP followed by an IPSP. Bath application of DhβE (green) reduces the EPSP. MLA (type I nAChR antagonist, 500 nM, orange) has no effect, but MEC (red) further reduced the EPSP.

(G) Effects of selective nAChR antagonists on the CIN-induced EPSP (one-way ANOVA, n = 13).

(H) Current-clamp recording of a THIN following CIN optogenetic stimulation. Atropine application (blue, 10 μM) abolishes the CIN-induced IPSP.

(I) IPSP reduction following atropine application (two-tailed paired t test, n = 5).

(J) Summary schematic showing the connectivity between CINs and THINs involving type II and (putative) type III nAChR responsible for the EPSP, as well as mAChRs involved in the slow IPSP.

*p < 0.05, **p < 0.01, ***p < 0.001; see text for exact p values. ns, non-significant.

amplitude of the EPSC following CINs optogenetic activation (−9.35 ± 5.66 pA [−14.1%]; p = 0.133, t = 1.652, two-tailed paired t test; n = 10; Figure S1G).

We then tested the involvement of mAChRs on the CIN-induced slow IPSC/P; atropine (10 μM) dramatically reduced the IPSC/P (−6 ± 1.72 pA [−69.77%]; p = 0.005, t = 3.496, n = 12, two-tailed paired t test; Figures 2H and 2I), demonstrating its muscarinic nature.

Atropine (10 μM) also significantly reduced the amplitude of the EPSP/C in SABIs (−12.9 ± 3.48 pA [−21.3%]; p = 0.0023, t = 3.71, n = 15, two-tailed paired t test; Figure S1H). However, this was not reproduced by application of another mAChR antagonist, scopolamine, which significantly increased the size of the EPSC (+10.34 ± 3.628 pA [+22.79%]; p = 0.015, t = 2.85, n = 12, two-tailed paired t test; Figure S1I), consistent with the blocking of the slow mAChR-mediated IPSC in SABIs.

These results demonstrate that CINs innervate striatal SABIs involving dual nAChR-mediated excitation and muscarinic-mediated slow inhibition (Figure 2J).

CIN innervation of low threshold spike interneurons (LTSIs)

Pharmacological and optogenetic studies indicate that mAChR activation inhibits low threshold spike interneurons (LTSIs; Elghaba et al., 2016; Melendez-Zaidi et al., 2019). The effect of nAChR activation in LTSIs seems dual with a direct excitatory effect through β2-nAChRs and an indirect inhibitory effect via increasing $GABA_A$ currents (Elghaba et al., 2016; Luo et al.,

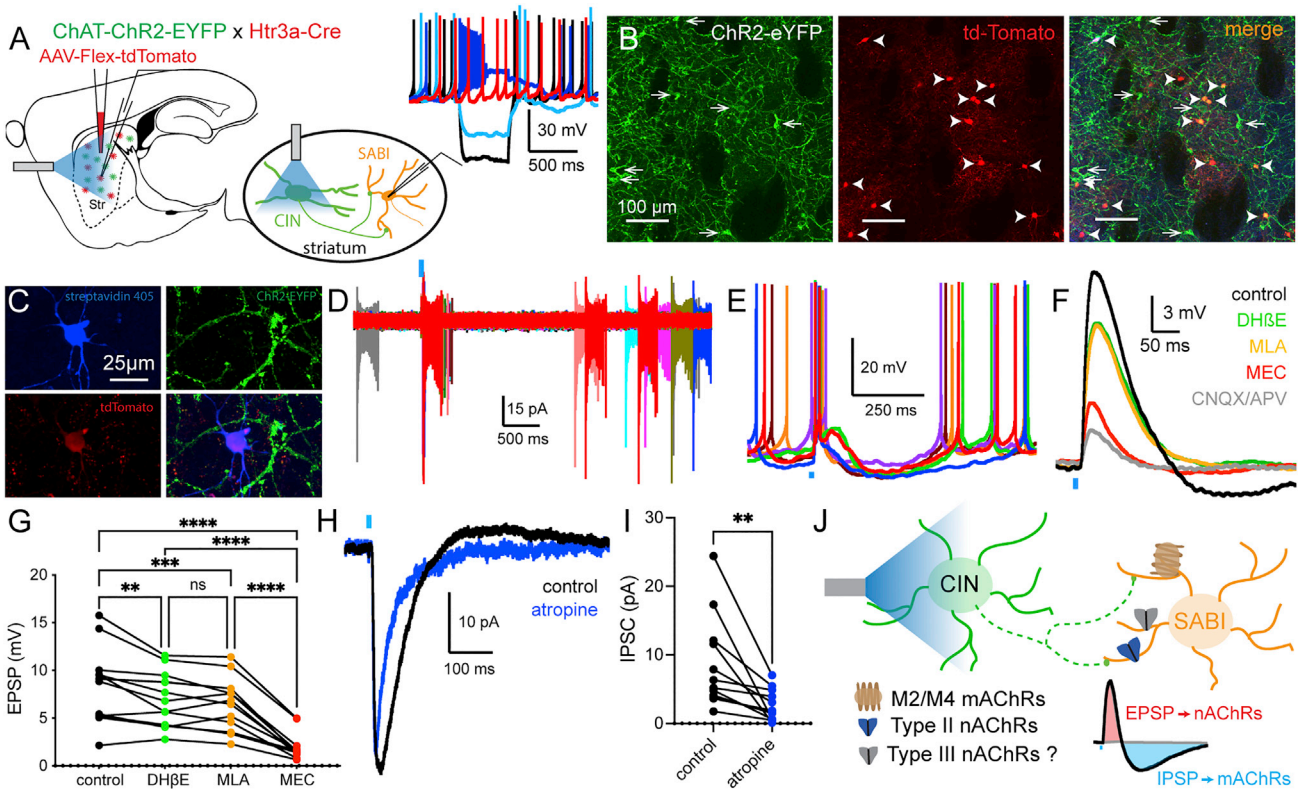

Figure 2. Cholinergic innervation of SABIs

(A) Schematic illustrating the experimental design using double-transgenic ChAT-ChR2-eYFP:Htr3a-Cre mice injected with a Cre-dependent td-Tomato AAV in the striatum. Inset: typical responses of a SABI to negative and positive somatic current injections.

(B) Confocal photomicrographs showing striatal transduction of Htr3a-Cre interneurons (red) and CINs (green).

(C) Confocal photomicrographs of a recorded SABI, filled with biocytin (streptavidin 405, blue) and surrounded by ChR2-expressing CIN cell body and processes (green).

(D) Cell-attached recording of a SABI showing spontaneous burst activity. The SABI responds to optogenetic stimulation of CINs (blue bar) with a large burst of APs.

(E) Current-clamp recording of a SABI firing APs in response to CIN stimulation.

(F) Current-clamp recording of a SABI following CIN optogenetic stimulation showing a large EPSP (black). Bath application of DhβE (1 μM, green) reduces the EPSP, MLA (500 nM, orange) has no effect, and MEC (5 μM, red) further reduced the EPSP.

(G) Quantification of the effect of selective nAChR antagonists on the CIN-induced EPSP (one-way ANOVA, n = 15).

(H) Voltage-clamp recording of a SABI following CIN optogenetic stimulation. Atropine application (blue, 10 μM) abolishes the CIN-induced IPSC.

(I) IPSC reduction following atropine application (two-tailed paired t test, n = 12).

(J) Summary schematic showing the connectivity between CINs and SABIs involving type II and putative type III nAChR responsible for the EPSP and mAChRs involved in the slow IPSP.

**p < 0.01, ***p < 0.001, ****p < 0.0001; see text for exact p values.

2013b; but see Munoz-Manchado et al., 2016). However, direct nAChR activation of LTSIs has not yet been shown using optogenetic stimulation of CINs (English et al., 2012; Melendez-Zaidi et al., 2019).

To examine the connectivity between CINs and LTSIs, we used double-transgenic ChAT-ChR2-eYFP::SST-Cre mice and transduced LTSIs with td-Tomato (N = 16 mice; Figures 3A–3C, S2A, and S2B). Optogenetic stimulation of CINs evokes a long pause response in LTSIs (Figures 3D and 3E) (Melendez-Zaidi et al., 2019). In some instances (~25%), the pause is followed by periods of burst activity as previously described (data not shown; Melendez-Zaidi et al., 2019). Consistent with a previous study, we demonstrate that the inhibition of LTSIs was mediated by mAChRs because it was blocked by atropine (10 μM; Figure 3D) (Melendez-Zaidi et al., 2019) (−7.75 ± 2.8 pA [−83.86%] versus control; p = 0.0252, two-tailed paired t test, t = 2.77; n = 5; Figures 3F, 3G, and S2C).

We observed that the pause is preceded by a small EPSP/C (−7.12 ± 1.19 pA, τ = 38.18 ± 5.25 ms, n = 25) sometimes sufficient to elicit AP firing (Figure 3E). Bath application of MEC almost completely abolished the CIN-induced EPSC (−3.37 ± 0.45 pA [−84.9%], two-tailed paired t test, t = 7.56, n = 9, p = 6.54×10^{-5}; Figures 3H and 3I), demonstrating the involvement of nAChRs. Interestingly, AMPA and NMDA receptor antagonists also significantly reduced the EPSC (10 μM CNQX and 10 μM APV, respectively; −10.3 ± 4.43 pA [−78.2%]; p = 0.04, paired t test, t = 2.327, n = 5; Figures 3J and 3K). Further, in some cells, we tested the impact of MEC applied after CNQX/APV.

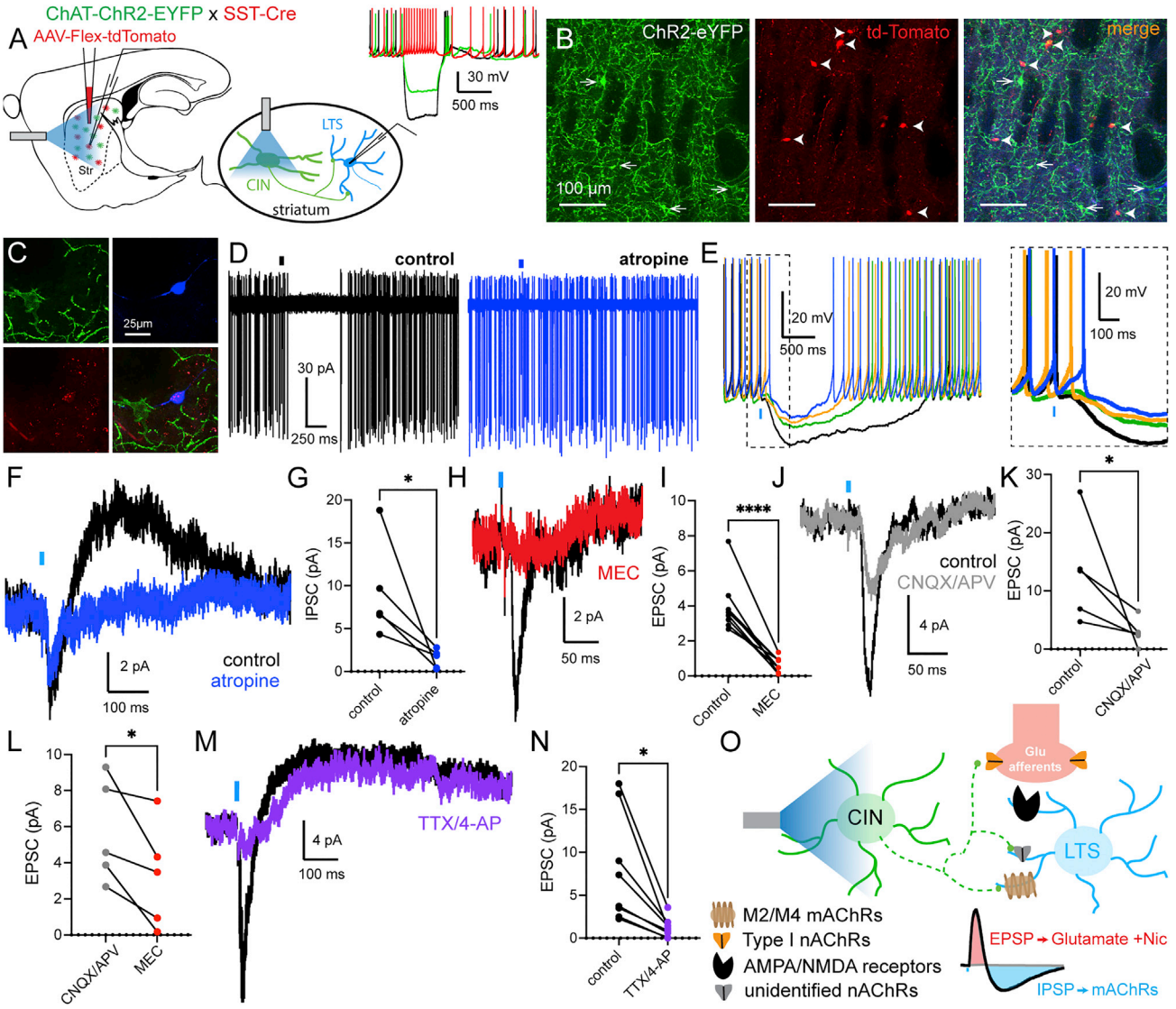

Figure 3. Cholinergic innervation of LTSIs

(A) Schematic illustrating the experimental design using double-transgenic ChAT-ChR2-eYFP:SST-Cre mice injected with a Cre-dependent td-Tomato AAV in the striatum. Inset: typical responses of a striatal LTSI to negative and positive somatic current injections.

(B) Left: confocal photomicrographs showing transduction of LTSIs (red) and CINs (green).

(C) Confocal photomicrographs of an LTSI, filled with biocytin (streptavidin 405, blue) and surrounded by ChR2-expressing axons/cells (green).

(D) Cell-attached recording of an LTSI showing spontaneous tonic activity. LTSI responds to optogenetic stimulation of CINs (blue bar) with a few APs followed by a long pause.

(E) Current-clamp recordings of a spontaneously active LTSI responding to CIN stimulation with an AP followed by a long pause. Right: enlargement of the dashed window, showing the excitation-inhibition sequence.

(F) Voltage-clamp recording of an LTSI. CIN stimulation evokes a modest EPSC followed by a slow IPSC (black trace, control). Application of atropine (10 μM, blue trace) almost completely abolishes the IPSC.

(G) IPSC reduction following atropine application (two-tailed paired t test, n = 5).

(H) Voltage-clamp recording of an LTSI showing that the CIN-induced EPSC is dramatically reduced by MEC (5 μM, red).

(I) EPSC reduction following MEC application (two-tailed paired t test, n = 9).

(J) Voltage-clamp recording of an LTSI showing that the CIN-induced EPSC is dramatically reduced by AMPA and NMDA antagonists (CNQX 10 μM and APV 10 μM, respectively, gray).

(K) EPSC reduction following CNQX/APV application (two-tailed paired t test, n = 5).

(L) Application of MEC significantly reduced the EPSC in comparison with CNQX/APV incubation (two-tailed paired t test, n = 5).

(legend continued on next page)

Subsequent application of MEC further reduced or completely abolished the remaining EPSCs ($p = 0.041$, $t = 2.97$, $n = 5$, two-tailed paired t test; Figure 3L). This suggests a mixed mechanism combining direct nAChR-mediated activation of LTSIs of moderate amplitude and a larger effect mediated by glutamate receptor activation. The next question was whether the glutamate component is due to nicotinic-induced glutamate release from cortical and/or thalamic afferents or by glutamate co-release from CINs (Nelson et al., 2014a). We recorded optogenetic responses in LTSIs under tetrodotoxin (TTX) + 4-aminopyridine (4-AP) to block polysynaptic responses, which dramatically reduced the EPSC amplitude (-6.71 ± 1.93 pA [-84.9%]; $p = 0.01$, $t = 3.47$, $n = 8$, two-tailed paired t test; Figures 3M and 3N). These results demonstrate that the mAChR-mediated slow kinetic IPSC is monosynaptic, but the glutamatergic component is polysynaptic, likely mediated by the activation of presynaptic nAChRs located on striatal afferents (Figure 3O).

Finally, we observed that bath application of CNQX/APV revealed longer-latency fast IPSCs in LTSIs following CIN optogenetic stimulation (Vh = −45 mV, 16/27; Figures S2C–S2F). These IPSCs are mediated by $GABA_A$ receptors because they can be abolished by a selective antagonist (bicuculline 10 μM; $p = 3.7 \times 10^{-6}$, $t = 7.09$, $n = 16$, two-tailed paired t test; Figures S2C–S2E). Given that CINs provide suprathreshold EPSP in THINs (see above) and that THINs innervate LTSIs (Assous et al., 2017), we hypothesize that these fast $GABA_A$ IPSCs likely involve this polysynaptic circuit (Figure S2F).

CIN innervation of FSIs

Presynaptic mAChR activation on FSIs has been shown to reduce the GABAergic inhibition on SPNs, whereas postsynaptic nAChR activation led to large depolarization in FSI (Koos and Tepper, 2002). However, in other studies, ACh agonist effects on FSIs were more moderate (Luo et al., 2013a) or non-existent (Munoz-Manchado et al., 2016).

To examine the responses of FSIs to optogenetic stimulation of CINs, we used double-transgenic ChAT-ChR2-eYFP::Htr3a-Cre mice and transduced Htr3a interneurons with td-Tomato ($N = 9$ mice; Figures 4A–4C and S3A). As mentioned, FSIs represent a large proportion of the Htr3a-transduced cells (Faust et al., 2015).

Optogenetic stimulation of CINs evoked a mixed excitatory/inhibitory response in FSIs revealed in current clamp recordings after eliciting AP firing by somatic current injection ($n = 10/15$ FSIs; Figures 4D and 4E). In voltage clamp, a 2-ms optical pulse elicited an EPSC (-44.24 ± 11.09 pA; $n = 16$; Figure 4F) with a fast decay time constant ($\tau = 5.44 \pm 0.65$ ms) consistent with the co-involvement of postsynaptic glutamate receptors (CNQX/APV: -40.51 ± 10.63 pA [-64.58%] versus control; $p = 0.0029$, $t = 3.81$, two-tailed paired t test; $n = 12$; Figures 4F–4H, S3B, and S3C), as well as postsynaptic nAChRs (MEC: -26.20 ± 7.28 pA [-86.53%] versus CNQX/APV condition; $p = 0.016$, $t = 3.6$, two-tailed paired t test, $n = 6$; Figures 4F–4H). MLA significantly reduced the EPSCs induced by CIN optogenetic activation (-8.19 ± 2.1 pA [-26%]; $p = 0.008$, $t = 3.89$, $n = 7$, two-tailed paired t test; Figures 4I and 4J) demonstrating the involvement of presynaptic nAChRs expressed by glutamatergic afferents. However, subsequent application of CNQX/APV further reduced the amplitude of the early EPSC (-18.54 ± 8.9 pA [-79.6%]; $p = 0.04$, $t = 2.09$, $n = 7$, two-tailed paired t test; Figures S3B and S3C), consistent with the existence of a direct glutamatergic input from CINs to FSIs (Nelson et al., 2014a) (Figure S3D).

The early EPSC is often followed by a slow IPSC ($n = 12/20$; 24.78 ± 10.02 pA; $\tau = 139.8 \pm 49.23$ ms; Figures 4K–4M) that exhibits properties consistent with $GABA_{Aslow}$ (Banks et al., 1998; English et al., 2012; Pearce, 1993; Tamas et al., 2003). Indeed, the CIN-induced IPSC is abolished by bicuculline (10 μM: -23.15 ± 10.08 pA [-93.42%]; $p = 0.04$, $t = 2.296$, two-tailed paired t test; $n = 13$; Figures 4K and 4L), and the decay time constant is increased by blocking GABA reuptake (NO711, 10 μM; $\tau_{control}$: 190.7 ± 55.9 ms, τ_{NO711}: 579.3 ± 100.7 ms [303.8% increase]; $n = 7$, $p = 0.0141$, $t = 3.423$, two-tailed paired t test; Figures 4K–4M). Given that NGFs are (so far) the only source of $GABA_{Aslow}$-mediated IPSCs in the striatum (Ibañez-Sandoval et al., 2011; Tepper et al., 2018), we hypothesize that the IPSC is due to the nAChR-mediated activation of NGFs (Figure 4Q) (English et al., 2012; Luo et al., 2013a).

Bath application of bicuculline revealed a late phase of EPSC barrages in a proportion of FSIs ($n = 6/12$ FSIs; Figures 4N–4Q). These asynchronous late EPSCs (amplitude: 21.77 ± 5.14 pA, charge transfer: 2.447 ± 1.09 pC; $n = 6$) could be blocked by glutamate receptor antagonists (CNQX/APV, 10 μM, [-90.2%]; $p = 0.0107$, $t = 3.964$, two-tailed paired t test; $n = 6$; Figures 4N–4P), suggesting the existence of tonic GABAergic inhibition of glutamatergic release from unidentified intrastriatal terminals that is triggered by ACh release from CINs.

Altogether, our results demonstrate a complex regulation of FSIs by CINs with (1) an initial fast excitation mediated by postsynaptic nAChRs, presynaptic nAChRs expressed by glutamatergic striatal afferents, and direct glutamate release by CINs; (2) a disynaptic slow inhibitory component likely involving CINs activation of NGFs; and (3) a late phase of glutamatergic EPSC barrages masked by tonic GABAergic inhibition (Figure 4Q).

Involvement of THINs and LTSIs in the disynaptic inhibition of SPNs

Optogenetic activation of CINs evokes a disynaptic inhibition of SPNs composed of distinct $GABA_{Afast}$ and $GABA_{Aslow}$ components (English et al., 2012; Faust et al., 2016; Nelson et al., 2014b). These compound IPSCs are due to activation of β2-nAChRs located on diverse striatal GINs. Although the $GABA_{Aslow}$ has been demonstrated to be due to activation of β2-nAChRs located on NGFs, the source of the $GABA_{Afast}$ current is still unclear but involves, at least partially, striatal GINs

(M) Voltage-clamp recording of an LTSI showing that the CIN-induced EPSC is dramatically reduced by TTX/4-AP (1 and 200 μM, respectively, purple).
(N) EPSC reduction following TTX/4-AP application (two-tailed paired t test, $n = 8$).
(O) Summary schematic showing the connectivity between CINs and LTSIs involving activation of postsynaptic nAChRs, presynaptic nAChRs activation of glutamatergic afferents, and postsynaptic mAChRs.
*$p < 0.05$, ****$p < 0.0001$; see text for exact p values.

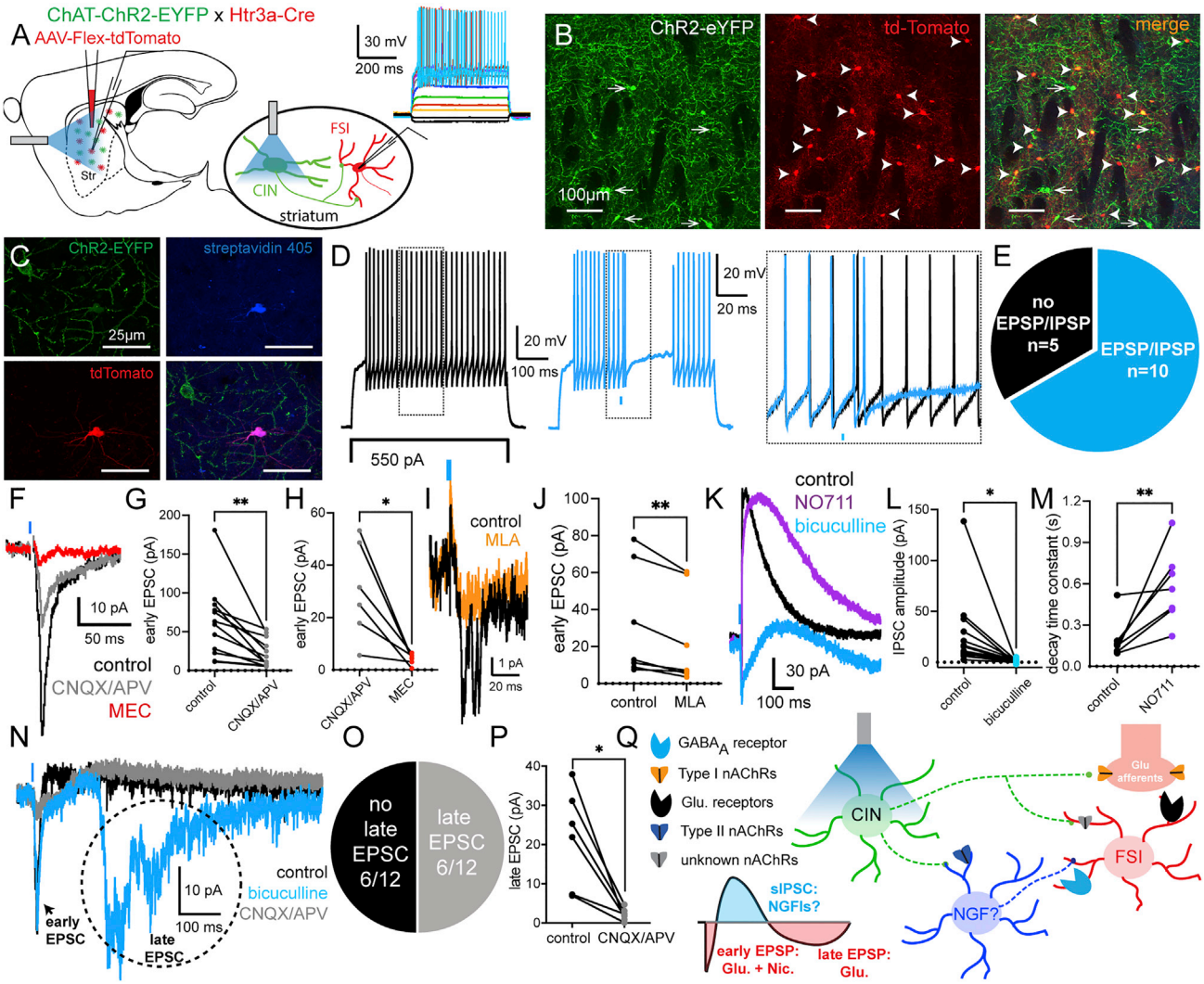

Figure 4. Cholinergic innervation of FSIs

(A) Schematic illustrating the experimental design using double-transgenic ChAT-ChR2-eYFP:Htr3a-Cre mice injected with a Cre-dependent td-Tomato AAV in the striatum. Inset: typical responses of an FSI to negative and positive somatic current injections.

(B) Confocal photomicrographs showing striatal transduction of Htr3a-Cre interneurons (red) and CINs (green).

(C) Confocal photomicrographs of a recorded FSI, filled with biocytin (streptavidin 405, blue) and surrounded by ChR2-expressing axons/cells (green).

(D) Left (black): large somatic current injection triggers AP firing in an FSI. Middle (blue): optogenetic stimulation of CINs evokes a brief increase in AP firing followed by a brief pause in firing. Right: enlargement around the optogenetic stimulation.

(E) Pie chart of the proportion of recorded FSIs responding to CIN optogenetic stimulation with sequential excitatory/inhibitory responses shown in (D).

(F) Voltage-clamp recording showing a CIN-induced EPSC in an FSI (black). The EPSC is significantly reduced by bath application of CNQX (10 μM, gray) and APV (10 μM, gray) and almost completely abolished by subsequent addition of MEC (5 μM, red).

(G) EPSC reduction following CNQX/APV application (two-tailed paired t test, n = 12).

(H) EPSC reduction following subsequent application of MEC (two-tailed paired t test, n = 6).

(I) The CIN-induced EPSC in FSI is significantly reduced by bath application of MLA (500 nM, orange).

(J) EPSC reduction following application of MLA (two-tailed paired t test, n = 7).

(K) When clamped at −45 mV, the majority of FSIs respond to CIN optogenetic stimulation with an IPSC following the EPSC (n = 12/20). The decay kinetics of the IPSC are significantly increased by application of the GABA transport blocker, NO711 (10 μM, purple), and completely abolished by bicuculline (10 μM, blue).

(L) IPSC reduction following application of bicuculline (two-tailed paired t test, n = 13).

(M) IPSC decay time constant following application of NO711 (two-tailed paired t test, n = 7).

(N) Application of bicuculline revealed a late excitatory phase.

(O) This was observed in n = 6/12 FSIs recorded in these conditions (Vh = −45 mV).

(P) These EPSC barrages can be blocked by bath application of CNQX 10 μM and APV 10 μM (gray, two-tailed paired t test, n = 6).

(Q) Summary schematic showing the connectivity between CINs and FSIs involving postsynaptic nAChRs, presynaptic nAChRs activation of striatal glutamatergic afferents, and disynaptic $GABA_{Aslow}$-mediated inhibition likely via CIN activation of NGFs.

*p < 0.05, **p < 0.01; see text for exact p values.

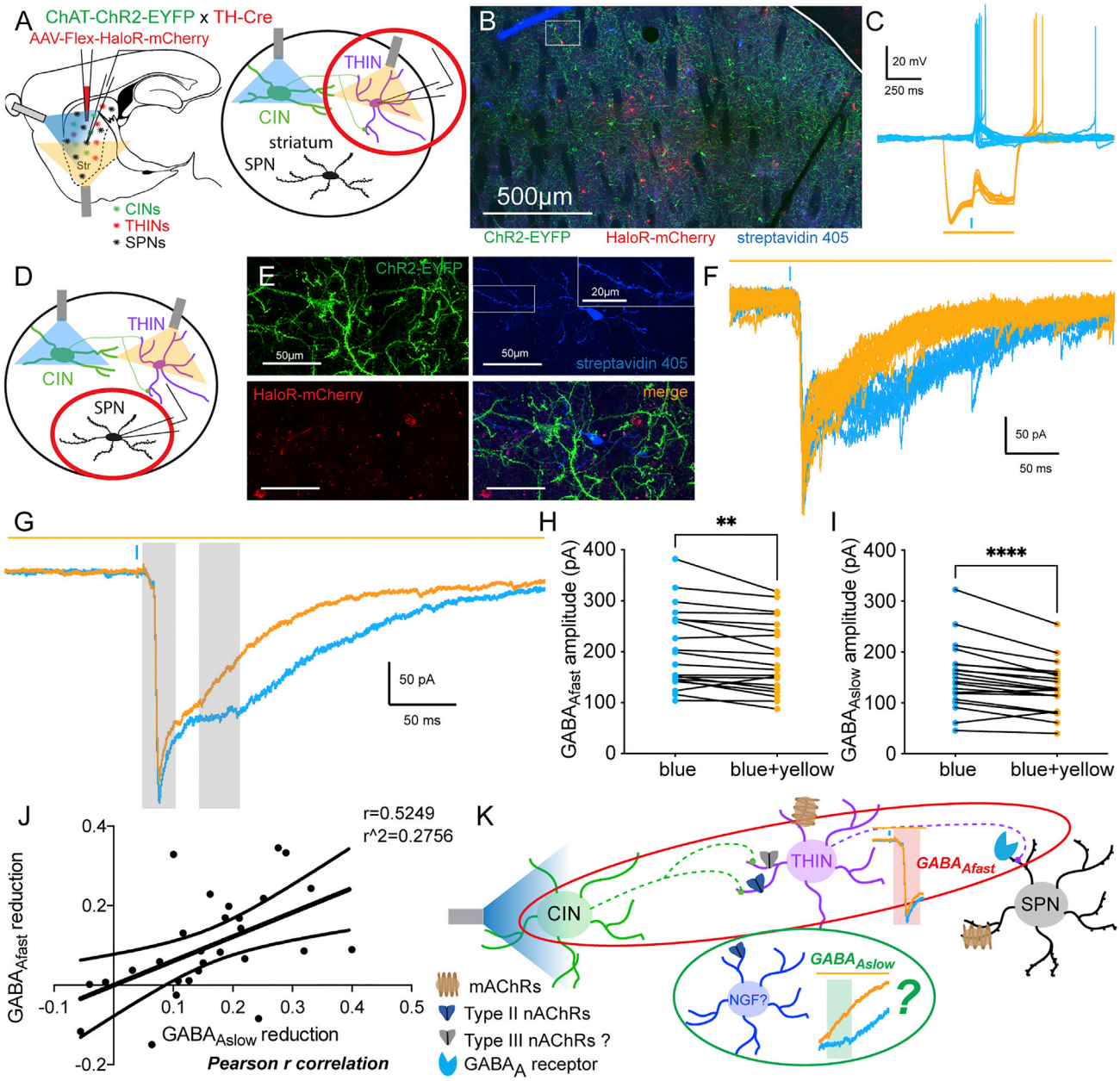

Figure 5. Influence of THINs in the nicotinic-mediated disynaptic inhibition of SPNs

(A) Schematic illustrating the experimental design using double-transgenic ChAT-ChR2-eYFP:TH-Cre mice injected with a Cre-dependent HaloR3.0 AAV in the striatum. This allows the optogenetic activation of CINs with blue light and the inhibition of THINs with yellow light.

(B) Confocal photomicrographs showing striatal transduction of THINs (red, HaloR3.0-mCherry) and CINs (green, ChR2-eYFP).

(C) Optogenetic activation of CINs with blue light evokes large depolarization and AP firing in a THIN (blue traces). Concomitant inhibition of THINs with yellow light (500 ms) evokes a large hyperpolarization preventing CIN-induced AP firing.

(D) Schematic illustrating the experimental design where recordings are obtained from SPNs while (1) activating CINs with blue light and (2) inhibiting THINs with yellow light.

(E) SPNs were filled with biocytin and revealed with streptavidin 405 nm (blue). Inset: enlargement of an SPN dendrite showing abundant spines.

(F and G) Optogenetic activation of CINs evokes large disynaptic compound IPSC in SPNs (recorded with $CsCl^{-}$ internal; see STAR methods), including a fast and a slow IPSC ($GABA_{Afast}$ and $GABA_{Aslow}$, respectively, blue traces). Concomitant inhibition of THINs induced a reduction in $GABA_{Afast}$ and $GABA_{Aslow}$ (F, examples of individual traces; G, average responses).

(H and I) Reduction of $GABA_{Afast}$ (H) and $GABA_{Aslow}$ (I) following optogenetic inhibition of THINs (two-tailed paired t test, n = 20).

(J) Linear regression and Pearson r analysis demonstrating that the reductions of $GABA_{Afast}$ and $GABA_{Aslow}$ are correlated.

(legend continued on next page)

targeted in the Htr3a-Cre mouse (English et al., 2012; Faust et al., 2016). Using an optogenetic approach in double-transgenic ChAT-ChR2::Htr3a-Cre mice injected with a Cre-dependent HaloR3.0 AAV, we were able to disconnect the CINs-Htr3a INs-SPNs cell circuit on a trial-by-trial basis and demonstrate the involvement of the Htr3a-targeted GINs in this circuit (Faust et al., 2016).

Here, we used a similar approach to test the involvement of LTSIs and THINs in this disynaptic circuit. First, we demonstrated that yellow light does not interfere with the disynaptic IPSCs measured in SPNs because there was no significant difference between blue light stimulation and blue + yellow light stimulation in ChAT-ChR2-eYFP mice (N = 5 mice; $GABA_{Afast}$: −7.98 ± 6.83 pA [−1.3%], p = 0.26, t = 1.17; $GABA_{Aslow}$: −5.04 ± 5.67 pA [−1.48%], p = 0.39, t = 0.89, n = 16, two-tailed paired t test; Figures S4A–S4E).

Next, we used double-transgenic ChAT-ChR2-eYFP:SST-Cre mice and transduced LTSIs with HaloR3.0 (N = 5 mice; Figures S5A–S5H). Stimulation of CINs evoked small-amplitude depolarization in LTSIs. Further, HaloR3.0-expressing LTSIs were strongly hyperpolarized by yellow light (590 nm; Figure S5C). The optogenetic inhibition of LTSIs did not significantly reduce the amplitude of either GABAergic current in SPNs ($GABA_{Afast}$: −20.98 ± 13.29 pA [−4.05%], p = 0.14, t = 1.58; $GABA_{Aslow}$: −6.37 ± 8.99 pA [−2.1%], p = 0.49, t = 0.71, n = 14, two-tailed paired t test; Figures S5D–S5H), demonstrating that LTSIs are not involved in this disynaptic circuit.

Then we tested the involvement of THINs using a similar approach. ChAT-ChR2-eYFP:TH-Cre mice were injected with a Flex-HaloR3.0 AAV (N = 11 mice; Figures 5A–5K). Optogenetic stimulation of CINs evoked AP firing in recorded THINs (n = 7; Figure 5C) consistent with the results described above (see Figure 1). On alternate trials, concomitant optogenetic inhibition of HaloR3.0-expressing THINs significantly hyperpolarized THINs and blocked AP firing in response to CIN stimulation (n = 7; Figure 5C), confirming the efficacy of the optogenetic approach. Next, we repeated the same stimulation protocol while recording from SPNs (Figures 5D and 5E). Yellow light illumination produced a small but significant reduction in the amplitude of the $GABA_{Afast}$ (−16.32 ± 4.64 pA [−7.95%]; p = 0.0023, t = 3.514, two-tailed paired t test; n = 20; Figures 5F–5H), demonstrating that THINs participate in this circuit. Surprisingly, the inhibition of THINs produces a more important reduction of the $GABA_{Aslow}$ (−22.37 ± 4.56 pA [−14.8%]; p = 9.7 × 10^{-5}, two-tailed paired t test; n = 20; Figures 5F, 5G, and 5I). This was unexpected because optogenetic activation of THINs does not evoke $GABA_{Aslow}$ responses in SPNs (Assous et al., 2018; Ibañez-Sandoval et al., 2010; Xenias et al., 2015). As mentioned above, the $GABA_{Aslow}$ in SPNs was attributed to CIN activation of NGFs. Interestingly, we found a significant correlation between the reduction of the $GABA_{Afast}$ and $GABA_{Aslow}$ components following inhibition of THINs (r = 0.52, r^2 = 0.28, p = 0.0041, Pearson r correlation; Figure 5J), suggesting a common mechanism. Given the ability of NGFs to form heterotypic gap junction with other interneurons in the cortex or hippocampus (Capogna, 2011; Olah et al., 2007; Simon et al., 2005; Zsiros and Maccaferri, 2005), we hypothesized that striatal NGFs may be electrically coupled with THINs, which could explain the reduction of $GABA_{Aslow}$ in SPNs following THINs inhibition (Figure 5K).

Electrical coupling between THINs and NGFs

We used TH-Cre:NPY-GFP mice injected with a AAV-Flex-ChR2 in the striatum (N = 7 mice; Figures 6A and 6B). The majority of NGFs (n = 17/28, 60.7%) respond to THIN stimulation with an EPSP/C (n = 17; Figures 6C–6F) that showed little or no variation in amplitude when THINs were optically stimulated with a pulse train (five pulses, 20 Hz, p1: 13.94 ± 1.95 pA, p2: 13.26 ± 1.78 pA, p3: 12.05 ± 1.61 pA, p4: 11.66 ± 1.64 pA, p5: 11.21 ± 1.52 pA; n = 14; Figures 6E and 6F) and a relatively slow decay time constant (τ: 25.21 ± 3.5 ms). Further, optogenetic activation of THINs evoked spikelets in NGFs (Figure 6D), and long optogenetic pulses (200 ms) induced sustained inward current in NGFs, all consistent with the existence of electrical coupling (Figure 6E). Finally, application of carbenoxolone (100 μM), which disrupts gap junction coupling (Connors, 2012), caused a significant reduction of the amplitude of the inward current measured in NGFs (p = 0.018; two-way ANOVA followed by Bonferroni's multiple comparisons test F(18,72) = 70.71; p < 10^{-6}; n = 10; Figures 6E and 6F). Further, we performed dual whole-cell recordings of THINs and NGFs and found that all tested pairs were reciprocally electrically connected (n = 3/3; Figures 6G and 6H).

Interestingly, these gap junctions are cell-type selective because THINs are not electrotonically coupled with LTSIs also targeted in the NPY-GFP mice (Table S1). Indeed, THIN optogenetic stimulation evokes powerful GABAergic IPSCs in most LTSIs (n = 7/9; data not shown; see Assous et al., 2017), further demonstrating the specificity of the striatal microcircuitry (Assous and Tepper, 2019; Tepper et al., 2018).

Altogether, these results indicate that the decrease in the CIN-induced $GABA_{Aslow}$ IPSCs in SPNs following the inhibition of THINs (and possibly $GABA_{Afast}$) is likely indirect, mediated by NGFs as a result of heterotypic electrical coupling.

Electrical coupling between THINs and NGFs and disynaptic inhibition of SPNs

Consistent with our data, carbenoxolone significantly reduced the amplitude of the $GABA_{Afast}$ and $GABA_{Aslow}$ components (N = 7 mice; Figures 7A–7E; $GABA_{Afast}$: −192 ± 36.7 pA [−62.5%], p = 4.7 × 10^{-5}, t = 5.23; $GABA_{Aslow}$: −191.6 ± 45.5 pA [−71.4%], p = 4.7 × 10^{-4}, t = 4.21, n = 20, two-tailed paired t test; Figures 7B–7D) demonstrating the importance of gap junctions in this disynaptic circuit. Interestingly, we found a significant correlation between the reduction of the $GABA_{Afast}$ and $GABA_{Aslow}$ components following carbenoxolone

(K) Summary schematic showing the role of THINs in the nAChR-mediated disynaptic inhibition of SPNs. Although our current circuit analysis provides a rationale for the involvement of THINs in the $GABA_{Afast}$-mediated IPSC, their involvement in the $GABA_{Aslow}$ component is more surprising and suggested to rely on CIN activation of NGFs.

**p < 0.01, ****p < 0.0001; see text for exact p values.

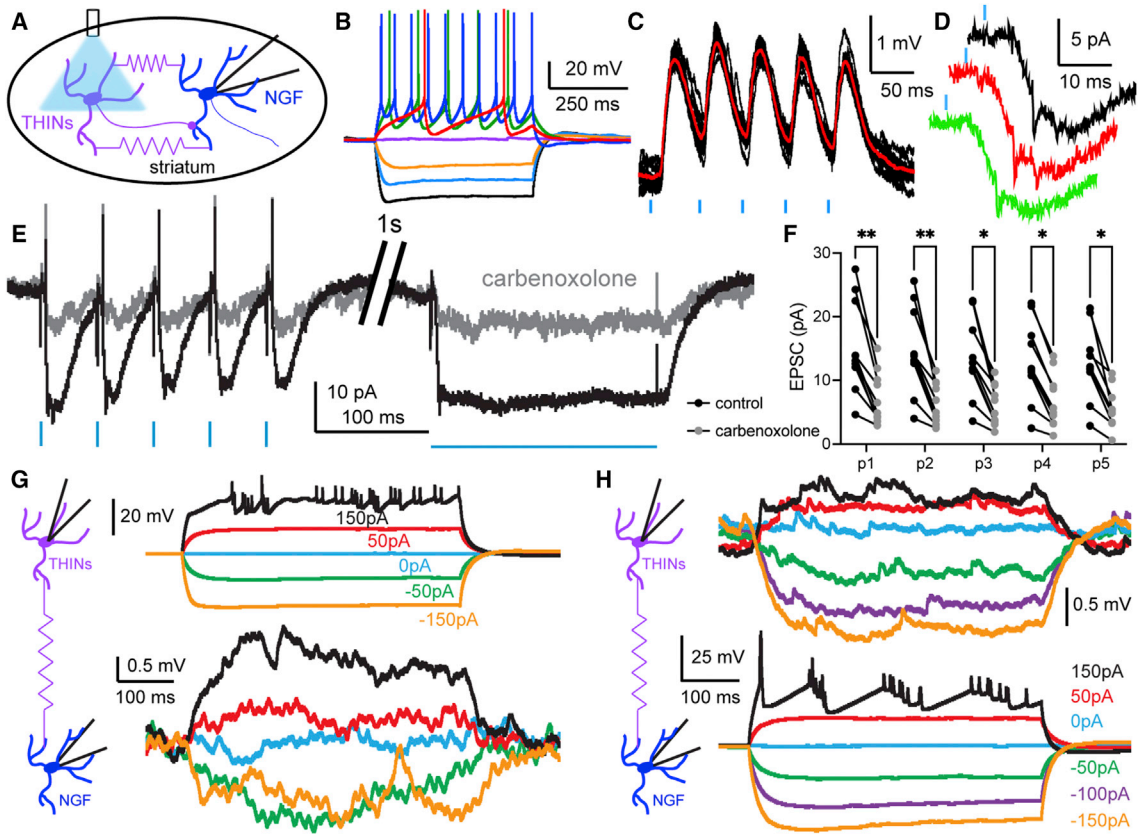

Figure 6. Electrical coupling between THINs and NGFs

(A) Schematic illustrating the experimental design using double-transgenic TH-Cre:NPY-GFP mice injected with a Cre-dependent ChR2 AAV in the striatum. This allows the optogenetic activation of THINs with blue light while recording from GFP-identified NGF interneurons.

(B) Typical response of an NGF interneuron to somatic current injection.

(C) THINs optogenetic stimulation evokes depolarization in an NGF (n = 17/28).

(D) Inward currents and "spikelets" recorded in an NGF following THIN optogenetic stimulation.

(E) THINs were optogenetically stimulated with a train of blue light pulses (5p, 20 Hz), followed by a single long optogenetic pulse (200 ms). NGF responded to the stimuli with inward currents that were dramatically reduced by carbenoxolone (100 μM, gray).

(F) Reduction of the THIN activation-induced EPSC following carbenoxolone application (two-way ANOVA, n = 10).

(G and H) Dual whole-cell recordings of THINs and NGFs in TH-Cre:NPY-GFP mice. (G) Negative and positive somatic current injection in a THIN triggered, respectively, hyperpolarization and depolarization in a connected NGF (n = 3). (H) Negative and positive somatic current injection in an NGF triggered, respectively, hyperpolarization and depolarization in an electrically coupled THIN (n = 3).

*p < 0.05, **p < 0.01; see text for exact p values.

application ($r = 0.877$, $r^2 = 0.77$, $p < 0.0001$, Pearson r correlation; Figure 7E), suggesting that both $GABA_{Afast}$ and $GABA_{Aslow}$ components involve gap junctions.

Then, we used a similar double-optogenetic approach as described in Figure 5, using ChAT-ChR2-eYFP:TH-Cre mice injected with a AAV-FlexHaloR3.0 (N = 5 mice). We measured that under carbenoxolone, THIN optogenetic inhibition no longer affected the disynaptic IPSCs measured in SPNs following optogenetic stimulation of CINs ($GABA_{Afast}$: +9.16 ± 7.6 pA [+7.9%], p = 0.24, t = 1.21, n = 20, two-tailed paired t test; $GABA_{Aslow}$: +8.45 ± 6.43 pA [+11%], p = 0.2, t = 1.32, n = 20, two-tailed paired t test; Figures 7F–7J). Further, we recorded some SPNs both pre-carbenoxolone and post-carbenoxolone (Figure S6). This confirmed our previous data demonstrating that THIN optogenetic inhibition significantly reduces both $GABA_{Afast}$ and $GABA_{Aslow}$ components pre-carbenoxolone ($GABA_{Afast}$: −32.77 ± 10.04 pA [−9.3%], p = 0.0098, t = 3.26; $GABA_{Aslow}$: −46.58 ± 20.29 pA [−14.7%], p = 0.047, t = 2.3, n = 10, two-tailed paired t test; Figures S6A–S6C), but not post-carbenoxolone ($GABA_{Afast}$: −0.004 ± 2.4 pA [−0%], p = 0.999, t = 0.002; $GABA_{Aslow}$: +3.34 ± 7.34 pA [+3.9%], p = 0.66, t = 0.45, n = 10, two-tailed paired t test; Figures S6B–S6D).

Finally, we compared traces in which we concomitantly activated CINs and inhibited THINs (blue + yellow) pre- and post-carbenoxolone (Figures S6E–S6H). Carbenoxolone significantly reduced the amplitude of the $GABA_{Afast}$ and $GABA_{Aslow}$ components ($GABA_{Afast}$: −186.6 ± 52.93 pA [−58.4%], p = 0.006, t = 3.53; $GABA_{Aslow}$: −181.8 ± 58.2 pA [−67.1%], p = 0.012, t = 3.13, n = 10, two-tailed paired t test; Figures S6G and S6H). Further, we found a significant correlation between the reduction of the $GABA_{Afast}$ and $GABA_{Aslow}$ components in this experiment ($r = 0.92$, $r^2 = 0.85$, $p = 0.0002$, Pearson r correlation; Figure S6I),

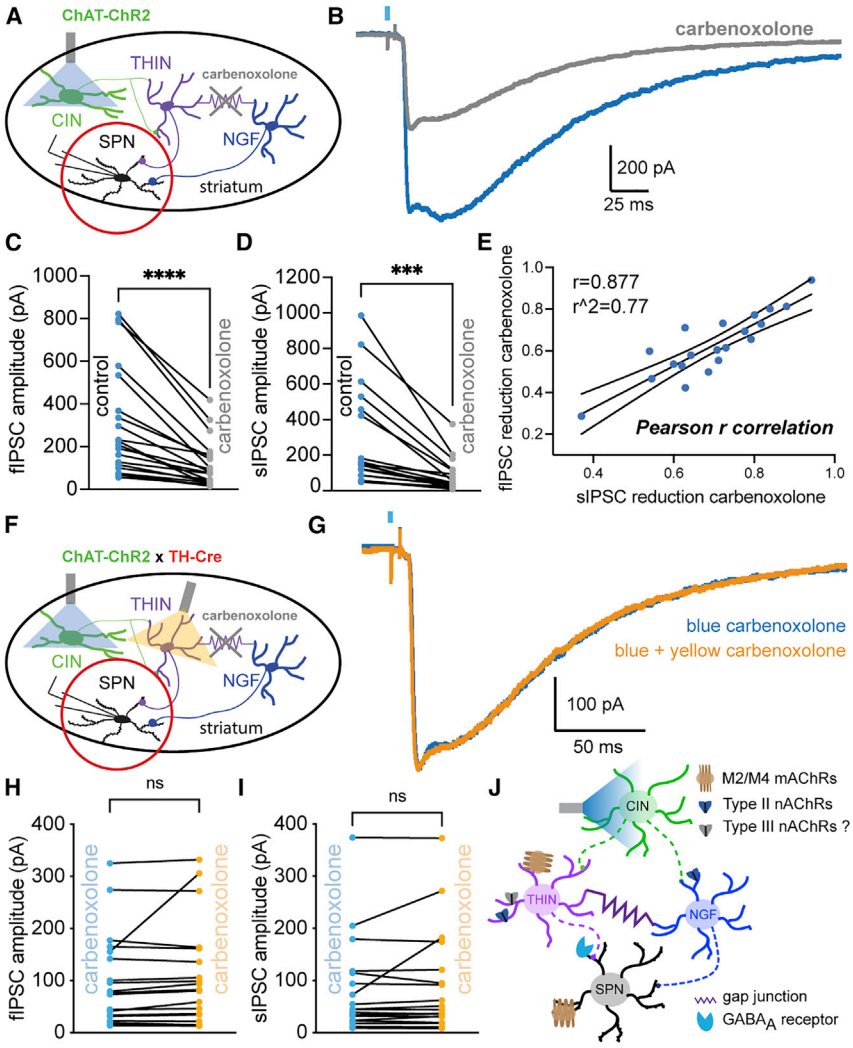

Figure 7. Role of electrical coupling in the disynaptic inhibition of SPNs

(A) Schematic illustrating the experimental design using ChAT-ChR2-eYFP mice and recording SPNs.

(B) Optogenetic activation of CINs evokes large disynaptic compound IPSC in SPNs comprising both $GABA_{Afast}$ and $GABA_{Aslow}$ (blue trace). Bath application of carbenoxolone (100 μM, gray trace) induced a reduction of both IPSCs.

(C and D) Reduction of $GABA_{Afast}$ (C) and $GABA_{Aslow}$ (D) following application of carbenoxolone (two-tailed paired t test, n = 20).

(E) Linear regression and Pearson r analysis demonstrating that the reduction of $GABA_{Afast}$ and $GABA_{Aslow}$ are correlated.

(F) Schematic illustrating the experimental design using ChAT-ChR2-eYFP:TH-Cre mice injected with a Cre-dependent HaloR3.0 AAV and recording from SPNs under carbenoxolone to block electrical coupling.

(G) Under carbenoxolone, optogenetic activation of CINs still evokes disynaptic compound IPSC in SPNs (blue trace), which are no longer affected by THIN optogenetic inhibition (orange trace).

(H and I) Lack of effect of THIN optogenetic inhibition on $GABA_{Afast}$ (H) and $GABA_{Aslow}$ (I) following application of carbenoxolone (two-tailed paired t test, n = 20).

(J) Summary schematic showing that the role of THINs in the CIN-induced disynaptic inhibition involves electrical coupling with NGFs.

***p < 0.001, ****p < 0.0001; see text for exact p values.

suggesting that the further reduction of the $GABA_{Afast}$ and $GABA_{Aslow}$ components would involve gap junctions. These results may imply that gap junctions other than the one linking the THINs and the NGF are involved in the disynaptic inhibition of SPNs.

DISCUSSION

Postsynaptic striatal nAChRs containing the β2 subunit, selectively expressed by striatal interneurons, are known to be involved in the powerful disynaptic inhibition of SPNs and play an important role in the regulation of striatal neuronal activity (English et al., 2012; Faust et al., 2016; Nelson et al., 2014b). Circuits dependent on these receptors provide a way for CINs to rapidly control striatal output after synchronization by a common excitatory afferent, such as the parafascicular nucleus (Aceves Buendia et al., 2019; Assous and Tepper, 2019; Oz et al., 2022; Rehani et al., 2019). However, the downstream intrastriatal circuitry and subtypes of GINs involved have not yet been precisely characterized. One reason has been the largely incomplete mapping and pharmacology of the interconnections between CINs and the diversity of striatal GINs and their intrastriatal connectomes. Here, we demonstrate that CINs innervate a large diversity of GINs involving different synaptic circuits and receptor subtypes. During this circuit analysis, we were able to test, using double optogenetics, the participation of the diverse populations of GINs in the disynaptic inhibition of SPNs induced by CIN population stimulation.

It has been shown previously that THINs express functional nAChRs because THINs respond strongly to local application of nicotinic agonists (Ibañez-Sandoval et al., 2015; Luo et al., 2013a). Further, using multiple simultaneous whole-cell recordings, it has been demonstrated that CINs directly innervate THINs (Dorst et al., 2020). Here, we demonstrate a dual control of THINs activity by CINs. Optogenetic stimulation of CINs evokes large suprathreshold nicotinic-mediated excitatory responses in THINs involving partially β2-nAChRs, as well as another subtype of nAChR distinct from the α7*-containing nAChR, possibly a β4*-containing nAChR (Ibañez-Sandoval et al., 2015; Luo et al., 2013a). Notably, the nicotinic EPSP is often followed by a mAChR-mediated IPSC/P responsible for a prolonged pause in THINs spontaneous activity. This demonstrates the existence of functional modulation of neuronal excitability via both nAChRs and mAChRs. This dual mechanism of

regulation of THINs activity by CINs should exert a large influence on intrastriatal functioning given the widespread targets of THINs (SPNs, LTSIs, CINs) (Assous et al., 2017, 2018; Dorst et al., 2020; Ibañez-Sandoval et al., 2010). Further, given the importance of other cholinergic systems in the generation of θ oscillation in the hippocampus, it is plausible that the oscillatory activity induced in several populations of interneurons by CINs could be responsible for the propagation of θ oscillations in the striatum whose source(s) is still unidentified (Lalla et al., 2017; Vandecasteele et al., 2014).

SABIs also receive suprathreshold nicotinic-mediated excitation after optogenetic stimulation of CINs. SABIs have been described as a population of interneurons selectively targeting other interneurons, but not SPNs (Assous et al., 2018), which could be compared with the VIP + interneurons in the cortex. VIP cortical interneurons also express nAChRs, and the resulting depolarization causes a disinhibition of principal neurons essential for the modulation of behavioral state (Fu et al., 2014). Although the functional role of the CIN innervation of SABIs remains to be elucidated, it is likely that the extreme bursting activity induced by CIN optogenetic stimulation is sufficient to silence the striatal targets of SABIs resulting in the disinhibition of SPNs (Assous et al., 2018). Disinhibition of SPNs has been suggested to play a role in transition from down state to up state and/or the creation of cell assemblies (Berke, 2011; Humphries, 2011; Lee et al., 2017; Plenz and Kitai, 1998).

Consistent with previous studies, we found that optogenetic stimulation of CINs evokes a long pause in the firing activity of LTSIs that is mediated principally by mAChR activation and a participation of $GABA_A$ receptors possibly via CIN activation of THINs (Assous et al., 2017; Elghaba et al., 2016; Frost Nylen et al., 2021; Hjorth et al., 2020; Melendez-Zaidi et al., 2019). Here, in addition to confirming these data, we also show the presence of an EPSC/P in most recorded LTSIs that involve both nAChRs and glutamate receptor activation. Although the nAChR activation is consistent with previous reports demonstrating β2-nAChR expression by LTSIs (Elghaba et al., 2016; Luo et al., 2013a), in addition we found that the glutamatergic response is due to the stimulation of presynaptic nAChRs on glutamatergic afferents.

Reports on CIN regulation of FSIs have been contradictory, where ACh application either evoked no postsynaptic responses (Munoz-Manchado et al., 2016), a slight depolarization (Luo et al., 2013a, 2013b), or a large depolarization (Koos and Tepper, 2002). Recently, it was demonstrated that tonic activation of nAChRs on FSIs participates in modulating corticostriatal feedforward inhibition by maintaining a GABAergic brake (Matityahu et al., 2022). Here, we showed a complex mechanism of regulation of FSIs by CINs where optogenetic activation of CINs triggers mixed excitatory/inhibitory responses in FSIs. Interestingly, we demonstrate that the glutamatergic component involves both the activation of presynaptic nAChR located on glutamatergic afferents and co-release of glutamate by CINs (Nelson et al., 2014a). Further, CIN optogenetic stimulation triggers $GABA_{Aslow}$-mediated inhibitory responses in the majority of FSIs, suggesting the involvement of NGFs. Indeed, these $GABA_{Aslow}$ responses have previously been observed only when studying the connectivity of NGFs with SPNs or CINs (English et al., 2012; Ibañez-Sandoval et al., 2011) and not for any other tested GINs. This would suggest that NGFs and FSIs would be reciprocally synaptically connected (Lee et al., 2017). Remarkably, incubation with a $GABA_A$ receptor antagonist revealed glutamatergic asynchronous EPSCs, suggesting the disinhibition and burst firing of striatal glutamatergic axons. Previous literature highlighted an important role of GABA in the regulation of corticostriatal glutamate release (Du et al., 2017; Logie et al., 2013; Paille et al., 2013). In addition, GABAergic transmission can control the temporal window of spiking of SPNs by regulating the generation and propagation of plateau potentials (Du et al., 2017). Interestingly, $GABA_{Aslow}$ originating from NGF interneurons were the most efficient for dendritic plateau inhibition in SPNs (Du et al., 2017). We propose that CIN activation of NGFs tonically inhibits corticostriatal terminals that densely innervate FSIs (Assous and Tepper, 2019; Koos and Tepper, 1999; Mallet et al., 2005). This mechanism may be important for prolonging the period of membrane depolarization and input integration in FSIs.

While investigating the influence of THINs in the disynaptic inhibition of SPNs following CIN optogenetic activation, we found that optogenetic inhibition of THINs elicits a significant decrease of both $GABA_{Afast}$ and $GABA_{Aslow}$ in SPNs. Our previous results demonstrate that THINs evoke $GABA_{Afast}$ only in SPNs (Assous et al., 2018; Ibañez-Sandoval et al., 2010; Xenias et al., 2015). Hence our present circuit analysis data support the involvement of the THINs in the disynaptic $GABA_{Afast}$ IPSC in SPNs, providing a mechanism through which THINs, under the influence of CINs, could rapidly regulate the activity of striatal outputs independently from any extrinsic cortical or thalamic input.

The reduction of $GABA_{Aslow}$ in SPNs following optogenetic inhibition of THINs was more surprising. Previously, the CIN-induced $GABA_{Aslow}$ in SPNs was attributed solely to CIN activation of NGF interneurons (English et al., 2012). Here, we demonstrate the existence of electrotonic coupling between NGFs and THINs. The pharmacological disruption of gap junctions abolishes the effect of THIN optogenetic inhibition on the fast and slow component, demonstrating the importance of electrical coupling in this nicotinic-mediated disynaptic circuit. Importantly, these results help clarify our previous data where we demonstrated that Htr3a-targeted GINs were involved in both the $GABA_{Afast}$ and the $GABA_{Aslow}$ component (Faust et al., 2016). Although the reduction of the slow component was attributed to NGF neurons, we could not explain the reduction of the fast component. Indeed, FSIs do not participate in this circuit (English et al., 2012; Nelson et al., 2014b), FAIs are also not involved (Faust et al., 2015) and SABIs do not significantly innervate SPNs (Assous et al., 2018), suggesting that NGFs could be necessary and sufficient to drive both the $GABA_{Afast}$ and $GABA_{Aslow}$ component. The data presented here reconcile these results demonstrating that electrotonic coupling between NGF and other populations of GINs, e.g., THINs, can explain (1) the reduction of the fast component reported previously (Faust et al., 2016) and (2) the reduction of the slow component demonstrated here. Interestingly, pharmacological disruption of gap junctions has an additional effect in comparison with inhibiting the THINs. This may suggest an insufficient inhibition of THINs

using this method. Instead, this could imply that other gap junctions are involved in the disynaptic inhibition of SPNs, including homotypic gap junctions between NGFs (English et al., 2012) and/or other heterotypic electrotonic coupling that is still undescribed. The existence of heterotypic gap junctions electrotonically linking NGFs and other striatal GINs suggests that NGFs are in position to control striatal network activity and could contribute to oscillatory activity by synchronizing interneuron networks as observed in cortical and hippocampal circuits (Overstreet-Wadiche and McBain, 2015; Zsiros et al., 2007; Zsiros and Maccaferri, 2005).

In contrast, we report that LTSIs are not involved in the disynaptic inhibition of SPNs following CINs optogenetic activation. This is consistent with the modest excitation of LTSIs by CINs and their lack of electrotonic coupling with THINs (Assous et al., 2017). Instead, LTSIs receive GABAergic innervation from THINs, demonstrating the intricacy and diversity of striatal interneuronal interconnections consisting of cell-type-selective chemical and electrotonic synapses (Assous et al., 2017).

Overall, our data demonstrate several complex and heterogeneous mechanisms of regulation of striatal GINs by CINs involving various subtypes of nAChRs, mAChRs, and glutamatergic and GABAergic receptors, as well as functional heterotypic electrotonic coupling. These results lay out valuable organizational principles of the synaptic organization among striatal interneurons where spontaneously active CINs would coordinate hierarchically the activity of GINs, thereby influencing striatal output activity. Further studies will be required to elucidate the role of these circuits in striatal-related functions (Abbondanza et al., 2022). Indeed, although CINs have been demonstrated to play an important role in behaviors such as reward processing and cognitive flexibility (Aoki et al., 2015; Apicella, 2017; Assous, 2021; Bradfield et al., 2013), as well as in associated neurological disorders including Parkinson's disease, obsessive-compulsive disorders, and Tourette syndrome, the involvement of specific subtypes of presynaptic and postsynaptic nAChRs is yet to be determined. A better understanding of striatal nAChR expression and function may lead to the development of targeted therapeutic approaches for the treatment of these prevalent BG-related disorders.

Limitations of the study

We demonstrated that THINs and SABIs seem to express mixed type II and type III nAChRs based on the partial blockade provided by DhβE. However, even though DhβE is considered a selective antagonist for type II nAChRs, it also inhibits other β2-nAChRs, including some type III nAChRs. Hence it is possible that these neurons express only type III nAChRs. Further, we found that atropine significantly reduces the fast nAChR-mediated EPSP/C in THINs and SABIs. However, these results were not reproduced with another non-specific mAChR antagonist (scopolamine), as well as by a selective M_1 mAChR antagonist (VU0255035, tested on THINs). These results highlight that at a micromolar concentration, atropine may also act as a channel blocker for nAChRs (Zwart and Vijverberg, 1997). Finally, we used carbenoxolone to demonstrate the existence of gap junctions between THINs and NGFs, which exhibit limited efficacy and selectivity (Connors, 2012). This is one of the reasons we also performed complex dual whole-cell recordings of these two rare GIN populations.

STAR★METHODS

Detailed methods are provided in the online version of this paper and include the following:

- KEY RESOURCES TABLE
- RESOURCE AVAILABILITY
  - Lead contact
  - Materials availability
  - Data and code availability
- EXPERIMENTAL MODEL AND SUBJECT DETAILS
- METHOD DETAILS
  - Intracerebral viral injection
  - Preparation of brain slices
  - Fluorescence and differential interference contrast imaging and recording
  - Drugs
  - Imaging
- QUANTIFICATION AND STATISTICAL ANALYSIS

SUPPLEMENTAL INFORMATION

Supplemental information can be found online at https://doi.org/10.1016/j.celrep.2022.111531.

ACKNOWLEDGMENTS

We thank Shubhi Yadav and Mina Nakhla for excellent technical assistance. This work was supported by National Institute of Neurological Disorders and Stroke (NINDS) grant R01 NS034865 (to J.M.T.), a NARSAD Young Investigator grant from the Brain and Behavior Research Foundation (to M.A.), a Rutgers Busch Biomedical grant (to M.A.), and Rutgers University.

AUTHOR CONTRIBUTIONS

M.A. and J.M.T. designed the study. M.A., S.K., and E.B.G. collected the electrophysiology data. F.S. participated in collecting anatomical data and managed the transgenic mice colony. M.A. wrote the first draft of the manuscript with major input from S.K. and J.M.T.

DECLARATION OF INTERESTS

The authors declare no competing interests.

INCLUSION AND DIVERSITY

We support inclusive, diverse, and equitable conduct of research.

Received: December 20, 2021
Revised: September 1, 2022
Accepted: September 29, 2022
Published: October 25, 2022

REFERENCES

Abbondanza, A., Ribeiro Bas, I., Modrak, M., Capek, M., Minich, J., Tyshkevich, A., Naser, S., Rangotis, R., Houdek, P., Sumova, A., et al. (2022). Nicotinic acetylcholine receptors expressed by striatal interneurons inhibit striatal activity and control striatal-dependent behaviors. J. Neurosci. *42*, 2786–2803.

Aceves Buendia, J.D.J., Tiroshi, L., Chiu, W.H., and Goldberg, J.A. (2019). Selective remodeling of glutamatergic transmission to striatal cholinergic interneurons after dopamine depletion. Eur. J. Neurosci. *49*, 824–833.

Albuquerque, E.X., Pereira, E.F.R., Alkondon, M., and Rogers, S.W. (2009). Mammalian nicotinic acetylcholine receptors: from structure to function. Physiol. Rev. *89*, 73–120.

Albuquerque, E.X., Pereira, E.F., Castro, N.G., Alkondon, M., Reinhardt, S., Schröder, H., and Maelicke, A. (1995). Nicotinic receptor function in the mammalian central nervous system. Ann. N. Y. Acad. Sci. *757*, 48–72.

Aoki, S., Liu, A.W., Zucca, A., Zucca, S., and Wickens, J.R. (2015). Role of striatal cholinergic interneurons in set-shifting in the rat. J. Neurosci. *35*, 9424–9431.

Apicella, P. (2017). The role of the intrinsic cholinergic system of the striatum: what have we learned from TAN recordings in behaving animals? Neuroscience *360*, 81–94.

Assous, M. (2021). Striatal cholinergic transmission. Focus on nicotinic receptors' influence in striatal circuits. Eur. J. Neurosci. *53*, 2421–2442.

Assous, M., Faust, T.W., Assini, R., Shah, F., Sidibe, Y., and Tepper, J.M. (2018). Identification and characterization of a novel spontaneously active bursty GABAergic interneuron in the mouse striatum. J. Neurosci. *38*, 5688–5699.

Assous, M., Kaminer, J., Shah, F., Garg, A., Koós, T., and Tepper, J.M. (2017). Differential processing of thalamic information via distinct striatal interneuron circuits. Nat. Commun. *8*, 15860.

Assous, M., and Tepper, J.M. (2019). Excitatory extrinsic afferents to striatal interneurons and interactions with striatal microcircuitry. Eur. J. Neurosci. *49*, 593–603.

Banks, M.I., Li, T.B., and Pearce, R.A. (1998). The synaptic basis of GABAA, slow. J. Neurosci. *18*, 1305–1317.

Bell, K.A., Shim, H., Chen, C.K., and McQuiston, A.R. (2011). Nicotinic excitatory postsynaptic potentials in hippocampal CA1 interneurons are predominantly mediated by nicotinic receptors that contain alpha4 and beta2 subunits. Neuropharmacology *61*, 1379–1388.

Berke, J.D. (2011). Functional properties of striatal fast-spiking interneurons. Front. Syst. Neurosci. *5*, 45.

Bradfield, L.A., Bertran-Gonzalez, J., Chieng, B., and Balleine, B.W. (2013). The thalamostriatal pathway and cholinergic control of goal-directed action: interlacing new with existing learning in the striatum. Neuron *79*, 153–166.

Campos, F., Alfonso, M., and Durán, R. (2010). In vivo modulation of alpha7 nicotinic receptors on striatal glutamate release induced by anatoxin-A. Neurochem. Int. *56*, 850–855.

Capogna, M. (2011). Neurogliaform cells and other interneurons of stratum lacunosum-moleculare gate entorhinal-hippocampal dialogue. J. Physiol. *589*, 1875–1883.

Connors, B.W. (2012). Tales of a dirty drug: carbenoxolone, gap junctions, and seizures. Epilepsy Curr. *12*, 66–68.

Dajas-Bailador, F., and Wonnacott, S. (2004). Nicotinic acetylcholine receptors and the regulation of neuronal signalling. Trends Pharmacol. Sci. *25*, 317–324.

Dani, J.A. (2001). Nicotinic receptor activity alters synaptic plasticity. Sci. World J. *1*, 393–395.

Dani, J.A., and Bertrand, D. (2007). Nicotinic acetylcholine receptors and nicotinic cholinergic mechanisms of the central nervous system. Annu. Rev. Pharmacol. Toxicol. *47*, 699–729.

Dannenberg, H., Young, K., and Hasselmo, M. (2017). Modulation of hippocampal circuits by muscarinic and nicotinic receptors. Front. Neural Circuits *11*, 102.

de Rover, M., Lodder, J.C., Kits, K.S., Schoffelmeer, A.N.M., and Brussaard, A.B. (2002). Cholinergic modulation of nucleus accumbens medium spiny neurons. Eur. J. Neurosci. *16*, 2279–2290.

Dorst, M.C., Tokarska, A., Zhou, M., Lee, K., Stagkourakis, S., Broberger, C., Masmanidis, S., and Silberberg, G. (2020). Polysynaptic inhibition between striatal cholinergic interneurons shapes their network activity patterns in a dopamine-dependent manner. Nat. Commun. *11*, 5113.

Du, K., Wu, Y.W., Lindroos, R., Liu, Y., Rózsa, B., Katona, G., Ding, J.B., and Kotaleski, J.H. (2017). Cell-type-specific inhibition of the dendritic plateau potential in striatal spiny projection neurons. Proc. Natl. Acad. Sci. USA *114*, E7612–E7621.

Elghaba, R., Vautrelle, N., and Bracci, E. (2016). Mutual control of cholinergic and low-threshold spike interneurons in the striatum. Front. Cell. Neurosci. *10*, 111.

English, D.F., Ibanez-Sandoval, O., Stark, E., Tecuapetla, F., Buzsáki, G., Deisseroth, K., Tepper, J.M., and Koos, T. (2012). GABAergic circuits mediate the reinforcement-related signals of striatal cholinergic interneurons. Nat. Neurosci. *15*, 123–130.

Faust, T.W., Assous, M., Shah, F., Tepper, J.M., and Koós, T. (2015). Novel fast adapting interneurons mediate cholinergic-induced fast GABAA inhibitory postsynaptic currents in striatal spiny neurons. Eur. J. Neurosci. *42*, 1764–1774.

Faust, T.W., Assous, M., Tepper, J.M., and Koós, T. (2016). Neostriatal GABAergic interneurons mediate cholinergic inhibition of spiny projection neurons. J. Neurosci. *36*, 9505–9511.

Frost Nylén, J., Carannante, I., Grillner, S., and Hellgren Kotaleski, J. (2021). Reciprocal interaction between striatal cholinergic and low-threshold spiking interneurons - a computational study. Eur. J. Neurosci. *53*, 2135–2148.

Fu, Y., Tucciarone, J.M., Espinosa, J.S., Sheng, N., Darcy, D.P., Nicoll, R.A., Huang, Z.J., and Stryker, M.P. (2014). A cortical circuit for gain control by behavioral state. Cell *156*, 1139–1152.

Gerfen, C.R., Paletzki, R., and Heintz, N. (2013). GENSAT BAC cre-recombinase driver lines to study the functional organization of cerebral cortical and basal ganglia circuits. Neuron *80*, 1368–1383.

Goldberg, J.A., Ding, J.B., and Surmeier, D.J. (2012). Muscarinic modulation of striatal function and circuitry. Handb. Exp. Pharmacol., 223–241.

Hjorth, J.J.J., Kozlov, A., Carannante, I., Frost Nylén, J., Lindroos, R., Johansson, Y., Tokarska, A., Dorst, M.C., Suryanarayana, S.M., Silberberg, G., et al. (2020). The microcircuits of striatum in silico. Proc. Natl. Acad. Sci. USA *117*, 9554–9565.

Humphries, M.D. (2011). Spike-train communities: finding groups of similar spike trains. J. Neurosci. *31*, 2321–2336.

Ibáñez-Sandoval, O., Tecuapetla, F., Unal, B., Shah, F., Koós, T., and Tepper, J.M. (2010). Electrophysiological and morphological characteristics and synaptic connectivity of tyrosine hydroxylase-expressing neurons in adult mouse striatum. J. Neurosci. *30*, 6999–7016.

Ibáñez-Sandoval, O., Tecuapetla, F., Unal, B., Shah, F., Koós, T., and Tepper, J.M. (2011). A novel functionally distinct subtype of striatal neuropeptide Y interneuron. J. Neurosci. *31*, 16757–16769.

Ibáñez-Sandoval, O., Xenias, H.S., Tepper, J.M., and Koós, T. (2015). Dopaminergic and cholinergic modulation of striatal tyrosine hydroxylase interneurons. Neuropharmacology *95*, 468–476.

Kaiser, S., and Wonnacott, S. (2000). alpha-bungarotoxin-sensitive nicotinic receptors indirectly modulate [(3)H]dopamine release in rat striatal slices via glutamate release. Mol. Pharmacol. *58*, 312–318.

Koós, T., and Tepper, J.M. (1999). Inhibitory control of neostriatal projection neurons by GABAergic interneurons. Nat. Neurosci. *2*, 467–472.

Koós, T., and Tepper, J.M. (2002). Dual cholinergic control of fast-spiking interneurons in the neostriatum. J. Neurosci. *22*, 529–535.

Lalla, L., Rueda Orozco, P.E., Jurado-Parras, M.T., Brovelli, A., and Robbe, D. (2017). Local or not local: investigating the nature of striatal theta oscillations in behaving rats. eNeuro *4*. ENEURO.0128, 17.2017.

Lee, K., Holley, S.M., Shobe, J.L., Chong, N.C., Cepeda, C., Levine, M.S., and Masmanidis, S.C. (2017). Parvalbumin interneurons modulate striatal output and enhance performance during associative learning. Neuron *93*, 1451–1463.e4.

Logie, C., Bagetta, V., and Bracci, E. (2013). Presynaptic control of corticostriatal synapses by endogenous GABA. J. Neurosci. *33*, 15425–15431.

Luo, R., Janssen, M.J., Partridge, J.G., and Vicini, S. (2013a). Direct and GABA-mediated indirect effects of nicotinic ACh receptor agonists on striatal neurones. J. Physiol. *591*, 203–217.

Luo, R., Partridge, J.G., and Vicini, S. (2013b). Distinct roles of synaptic and extrasynaptic GABAAreceptors in striatal inhibition dynamics. Front. Neural Circuits *7*, 186.

Mallet, N., Le Moine, C., Charpier, S., and Gonon, F. (2005). Feedforward inhibition of projection neurons by fast-spiking GABA interneurons in the rat striatum in vivo. J. Neurosci. *25*, 3857–3869.

Matityahu, L., Malgady, J.M., Schirelman, M., Johansson, Y., Wilking, J.A., Silberberg, G., Goldberg, J.A., and Plotkin, J.L. (2022). A tonic nicotinic brake controls spike timing in striatal spiny projection neurons. Elife *11*, e75829.

Melendez-Zaidi, A.E., Lakshminarasimhah, H., and Surmeier, D.J. (2019). Cholinergic modulation of striatal nitric oxide-producing interneurons. Eur. J. Neurosci. *50*, 3713–3731.

Mesulam, M.M., Mufson, E.J., Levey, A.I., and Wainer, B.H. (1984). Atlas of cholinergic neurons in the forebrain and upper brainstem of the macaque based on monoclonal choline acetyltransferase immunohistochemistry and acetylcholinesterase histochemistry. Neuroscience *12*, 669–686.

Muñoz-Manchado, A.B., Foldi, C., Szydlowski, S., Sjulson, L., Farries, M., Wilson, C., Silberberg, G., and Hjerling-Leffler, J. (2016). Novel striatal GABAergic interneuron populations labeled in the 5HT3a(EGFP) mouse. Cereb. Cortex *26*, 96–105.

Nelson, A.B., Bussert, T.G., Kreitzer, A.C., and Seal, R.P. (2014a). Striatal cholinergic neurotransmission requires VGLUT3. J. Neurosci. *34*, 8772–8777.

Nelson, A.B., Hammack, N., Yang, C.F., Shah, N.M., Seal, R.P., and Kreitzer, A.C. (2014b). Striatal cholinergic interneurons Drive GABA release from dopamine terminals. Neuron *82*, 63–70.

Oláh, S., Komlósi, G., Szabadics, J., Varga, C., Tóth, E., Barzó, P., and Tamás, G. (2007). Output of neurogliaform cells to various neuron types in the human and rat cerebral cortex. Front. Neural Circuits *1*, 4.

Overstreet-Wadiche, L., and McBain, C.J. (2015). Neurogliaform cells in cortical circuits. Nat. Rev. Neurosci. *16*, 458–468.

Oz, O., Matityahu, L., Mizrahi-Kliger, A., Kaplan, A., Berkowitz, N., Tiroshi, L., Bergman, H., and Goldberg, J.A. (2022). Non-uniform distribution of dendritic nonlinearities differentially engages thalamostriatal and corticostriatal inputs onto cholinergic interneurons. Elife *11*, e76039.

Paille, V., Fino, E., Du, K., Morera-Herreras, T., Perez, S., Kotaleski, J.H., and Venance, L. (2013). GABAergic circuits control spike-timing-dependent plasticity. J. Neurosci. *33*, 9353–9363.

Pearce, R.A. (1993). Physiological evidence for two distinct GABAA responses in rat hippocampus. Neuron *10*, 189–200.

Plenz, D., and Kitai, S.T. (1998). Up and down states in striatal medium spiny neurons simultaneously recorded with spontaneous activity in fast-spiking interneurons studied in cortex-striatum-substantia nigra organotypic cultures. J. Neurosci. *18*, 266–283.

Rehani, R., Atamna, Y., Tiroshi, L., Chiu, W.H., de Jesús Aceves Buendía, J., Martins, G.J., Jacobson, G.A., and Goldberg, J.A. (2019). Activity patterns in the neuropil of striatal cholinergic interneurons in freely moving mice represent their collective spiking dynamics. eNeuro *6*. ENEURO.0351, 18.2018.

Rice, M.E., and Cragg, S.J. (2004). Nicotine amplifies reward-related dopamine signals in striatum. Nat. Neurosci. *7*, 583–584.

Simon, A., Oláh, S., Molnár, G., Szabadics, J., and Tamás, G. (2005). Gap-junctional coupling between neurogliaform cells and various interneuron types in the neocortex. J. Neurosci. *25*, 6278–6285.

Sullivan, M.A., Chen, H., and Morikawa, H. (2008). Recurrent inhibitory network among striatal cholinergic interneurons. J. Neurosci. *28*, 8682–8690.

Tamás, G., Lorincz, A., Simon, A., and Szabadics, J. (2003). Identified sources and targets of slow inhibition in the neocortex. Science *299*, 1902–1905.

Tepper, J.M., Koós, T., Ibanez-Sandoval, O., Tecuapetla, F., Faust, T.W., and Assous, M. (2018). Heterogeneity and diversity of striatal GABAergic interneurons: update 2018. Front. Neuroanat. *12*, 91.

Vandecasteele, M., Varga, V., Berényi, A., Papp, E., Barthó, P., Venance, L., Freund, T.F., and Buzsáki, G. (2014). Optogenetic activation of septal cholinergic neurons suppresses sharp wave ripples and enhances theta oscillations in the hippocampus. Proc. Natl. Acad. Sci. USA *111*, 13535–13540.

Witten, I.B., Lin, S.C., Brodsky, M., Prakash, R., Diester, I., Anikeeva, P., Gradinaru, V., Ramakrishnan, C., and Deisseroth, K. (2010). Cholinergic interneurons control local circuit activity and cocaine conditioning. Science *330*, 1677–1681.

Xenias, H.S., Ibáñez-Sandoval, O., Koós, T., and Tepper, J.M. (2015). Are striatal tyrosine hydroxylase interneurons dopaminergic? J. Neurosci. *35*, 6584–6599.

Zhang, H., and Sulzer, D. (2004). Frequency-dependent modulation of dopamine release by nicotine. Nat. Neurosci. *7*, 581–582.

Zhou, F.M., Liang, Y., and Dani, J.A. (2001). Endogenous nicotinic cholinergic activity regulates dopamine release in the striatum. Nat. Neurosci. *4*, 1224–1229.

Zhou, F.M., Wilson, C.J., and Dani, J.A. (2002). Cholinergic interneuron characteristics and nicotinic properties in the striatum. J. Neurobiol. *53*, 590–605.

Zsiros, V., Aradi, I., and Maccaferri, G. (2007). Propagation of postsynaptic currents and potentials via gap junctions in GABAergic networks of the rat hippocampus. J. Physiol. *578*, 527–544.

Zsiros, V., and Maccaferri, G. (2005). Electrical coupling between interneurons with different excitable properties in the stratum lacunosum-moleculare of the juvenile CA1 rat hippocampus. J. Neurosci. *25*, 8686–8695.

Zwart, R., and Vijverberg, H.P. (1997). Potentiation and inhibition of neuronal nicotinic receptors by atropine: competitive and noncompetitive effects. Mol. Pharmacol. *52*, 886–895.

STAR★METHODS

KEY RESOURCES TABLE

REAGENT or RESOURCE	SOURCE	IDENTIFIER
Antibodies		
Streptavidin, Alexa Fluor™ 405 conjugate	Thermo Fischer Scientific	Cat#: S32351
Rabbit Polyclonal anti-GFP, Alexa Fluor™ 488	Thermo Fischer Scientific	Cat#: A-21311; RRID:AB_221477
Bacterial and virus strains		
pAAV-FLEX-tdTomato	Edward Boyden	Addgene viral prep # 28306-AAV5; RRID:Addgene_28306
pAAV-EF1α-double floxed-hChR2(H134R)-mCherry-WPRE-HGHpA	Karl Deisseroth	Addgene viral prep # 20297-AAV5; RRID:Addgene_20297
AAV-EF1α-DIO-eNpHR3.0-mCherry-WPRE(AAV5)	University of North Carolina at Chapel Hill (Karl Deisseroth)	N/A
Chemicals, peptides, and recombinant proteins		
Alexa Fluor™ 594 Hydrazide	Thermo Fischer Scientific	Cat#: A10438
Biocytin	Sigma-Aldrich	Cat#: B4261; CAS: 576-19-2
Dihydro-β-erythroidine hydrobromide	Tocris	Cat#: 2349; CAS: 29734-68-7
Methyllycaconitine citrate salt	Sigma-Aldrich	Cat#: M168; CAS: 112825-05-5
Mecamylamine hydrochloride	Tocris	Cat#: 2843; CAS: 110691-49-1
Atropine methyl nitrate	Sigma-Aldrich	Cat#: A0382; CAS: 52-88-0
Scopolamine hydrobromide	Tocris	Cat#: 1414; CAS: 114-49-8
VU 0255035	Tocris	Cat#: 3727; CAS: 1135243-19-4
NO-711 hydrochloride	Sigma-Aldrich	Cat#: N142; CAS: 145645-62-1
1(S),9(R)-(−)-Bicuculline methiodide	Sigma-Aldrich	Cat#: 14343; CAS: 40709-69-1
CNQX disodium salt	Tocris	Cat#: 1045; CAS: 479347-85-8
DL-APV	Tocris	Cat#: 0105; CAS: 76326-31-3
Tetrodotoxin	Sigma-Aldrich	Cat#: T8024; CAS: 4368-28-9
4-Aminopyridine	Sigma-Aldrich	Cat#: A0152; CAS: 504-24-5
Experimental models: Organisms/strains		
Mouse: B6.Cg-Tg(Chat-COP4* H134R/EYFP,Slc18a3) 6Gfng/J	The Jackson Laboratory	Strain #:014546; RRID:IMSR_JAX:014546
Mouse: $Sst^{tm2.1(cre)Zjh}$/J	The Jackson Laboratory	Strain #:013044; RRID:IMSR_JAX:013044
Mouse: B6.FVB-Tg(Npy-hrGFP)1Lowl/J	The Jackson Laboratory	Strain #:006417; RRID:IMSR_JAX:006417
Mouse: Tg(Th-cre)FI12Gsat/Mmucd	MMRRC	017262-UCD; RRID:MMRRC_017262-UCD
Mouse: Tg(Htr3a-cre)NO152Gsat/Mmucd	MMRRC	036680-UCD; RRID:MMRRC_036680-UCD
Software and algorithms		
GraphPad Prism 9	GraphPad Software	RRID:SCR_002798; http://www.graphpad.com/
Signal 7	Cambridge Electronic Device	RRID:SCR_014276; http://ced.co.uk/products/signal
Axograph Version 1.7.6	AxoGraph	RRID:SCR_014284: https://axograph.com
Adobe Illustrator CS	Adobe	RRID:SCR_010279 https://www.adobe.com/products/illustrator.html

RESOURCE AVAILABILITY

Lead contact

Further information and requests for resources and reagents should be directed to and will be fulfilled by the lead contact, Maxime Assous (assous.maxime@gmail.com).

Materials availability

This study did not generate new unique reagents.

Data and code availability

- All data reported in this paper will be shared by the lead contact upon request.
- This paper does not report original code.
- Any additional information required to reanalyze the data reported in this paper is available from the lead contact upon request.

EXPERIMENTAL MODEL AND SUBJECT DETAILS

All procedures used in this study were performed in accord with the National Institutes of Health Guide to the Care and Use of Laboratory Animals and with the approval of the Rutgers University Institutional Animal Care and Use Committee.

Subjects were adult male and female mice, 3–6 months of age. ChAT-ChR2-eYFP mice (Tg(Chat-COP4*H134R/eYFP,Slc18a3)6Gfng/J; Jackson Labs, Bar Harbor, MA, USA) were crossed with either 1) BAC transgenic TH–Cre [Tg(TH–Cre)12Gsat; Gene Expression Nervous System Atlas (GENSAT) 2) Htr3a-Cre mice [(Tg (HTR3a-Cre)NO152Gsat/Mmucd, MMRRC, University of California, Davis, (Gerfen et al., 2013)], or 3) SST-Cre mice (Sst-IRES-Cre, Stock No: 013044, The Jackson laboratory). To test the presence of electrical coupling between THINs and NGF interneurons we used double transgenic TH–Cre crossed with (BAC) transgenic mice that express the humanized Renilla green fluorescent protein (hrGFP) (Stratagene) under the control of the mouse NPY promoter (NPY-GFP, stock 006417; The Jackson Laboratory, Table S1). Double transgenic mice (ChAT-ChR2-eYFP::TH-Cre, ChAT-ChR2-eYFP::Ht3ra-Cre, ChAT-ChR2-eYFP::SST-Cre and TH-Cre::NPY-GFP) were genotyped and those found to be positive for both transgenes of interest were used for all recordings. Mice were housed in groups of up to four per cage and maintained on a 12-h light cycle with ad libitum access to food and water.

METHOD DETAILS

Intracerebral viral injection

The surgery and viral injections took place inside a Biosafety Level-2 isolation hood. Mice were anesthetized with isoflurane (1–2.5%, delivered with O2, 1 L/min) and mounted in a stereotaxic frame. Bupivacaine was injected under the scalp for local anesthesia at the site of the surgery. Coordinates to target the striatum were 0.6 mm anterior and 1.9 mm lateral to bregma. A replication non competent adeno-associated virus (AAV5-CAG-Flex-td-Tomato, University of North Carolina, Vector Core Services, Chapel Hill, NC or AAV5-EF1α-DIO-epNHR3.0-mCherry, Penncore or AAV5-EF1α-DIO-hChR2(H134R)-mCherry, University of North Carolina, Vector Core Services, Chapel Hill, NC) was delivered by glass pipette to two sites, -2.5 mm and $-3'.0$ mm ventral to brain surface, for a total volume of 0.8 μL at 9.2 nL/5sec using a Nanoject II Auto-Nanoliter Injector (Drummond Scientific Company). Following viral delivery the pipette was left in place for 10 min before being slowly retracted. Mice were then treated with ketoprofen and buprenorphine for analgesia. Expression of the viral transgene was allowed for at least 4 weeks before animals were used for histology or physiology.

Preparation of brain slices

Adult mice (3–6 months old) were deeply anesthetized with an intraperitoneal injection of 80 mg/kg ketamine and 20 mg/kg xylazine before being transcardially perfused with ice-cold N-methyl D-glucamine (NMDG)-based solution containing (in mM): 103.0 NMDG, 2.5 KCl, 1.2 NaH2PO4, 30.0 NaHCO3, 20.0 HEPES, 25.0 Glucose, 101.0 HCl, 10.0 MgSO4, 2.0 Thiourea, 3.0 sodium pyruvate, 12.0 N-acetyl cysteine and 0.5 CaCl2 saturated with 95% O2 and 5% CO2, pH 7.2–7.4. After decapitation, the brain was quickly removed into a beaker containing the ice-cold oxygenated NMDG-based solution before obtaining 300 μm parahorizontal slices using a vibratome (VT1200S; Leica Microsystems). Sections were immediately transferred to recover in well oxygenated NMDG-based solution at 35°C for 5 min, after which they were transferred to well-oxygenated normal Ringer's solution at 25°C until placed in the recording chamber constantly perfused (2–4 mL/min) with oxygenated Ringer's solution at 32–34°C. Drugs were dissolved freshly each day in Ringer's solution and applied in the perfusion medium.

Fluorescence and differential interference contrast imaging and recording

For recording striatal interneurons transduced with fluorescent AAV, slices were initially visualized under epifluorescence illumination with a digital frame transfer camera (Cooke SensiCam) mounted on an Olympus BX50-WI epifluorescence microscope with a 40X long working distance water-immersion lens. Once a fluorescent interneuron was identified, visualization was switched to

infrared–differential interference contrast microscopy for patching the neuron. Micropipettes for whole-cell recording were constructed from 1.2 mm outer diameter borosilicate pipettes on a Narishige PP-83 vertical puller. The standard internal solution for whole-cell current-clamp recording of interneurons was as follows (in mM): 130 K-gluconate, 10 KCl, 2 MgCl2, 10 HEPES, 4 Na_2ATP, 0.4 Na_2GTP, pH 7.3. For recording the disynaptic inhibition of SPNs following optogenetic stimulation of CINs we used a $CsCl^-$-based internal solution containing the following (in mM): 125 $CsCl^-$, 0.1 EGTA, 10 HEPES, 2 MgCl2, 4 Na2ATP, and 0.4 Na2GTP. This solution also contained 0.2% Alexa Fluor 594 (Molecular Device), or biocytin (Sigma) to verify the identity of SPNs and interneurons. Pipettes had a DC impedance of 3–5 MΩ. Membrane currents and potentials were recorded using an Axoclamp 700B amplifiers (Molecular Devices). Recordings were digitized at 20 kHz with a CED Micro 1401 Mk II and a PC running Signal, version 5 (Cambridge Electronic Design). Optogenetic stimulation was performed using a high power Multi LED (LZC-R0H100-0000, mouser). Stimulation of channelrhodopsin-2 (ChR2)-expressing neurons *ex vivo* consisted of 2 ms duration blue light pulses (450 nm). Optogenetic stimulation of halorhodopsin (HaloR3.0) consisted of 700 ms duration yellow light pulses (590 nm) starting 200 ms before the blue light pulse. Optogenetic pulses were delivered at 30 s intervals.

Drugs

We used bicuculline (10 μM, Sigma) to block $GABA_A$ receptors. Dihydro-β-erythroidine hydrobromide (DhβE; 1 μM, Tocris) was used to block nAChRs that contain β2-subunits including Type 2 nicotinic receptors (α4β2), and some heterormeric Type III nAChRs (β2*-containing). Methyllycaconitine citrate (MLA; 500 nM, Tocris) was used as an antagonist of nAChRs containing the α7 subunit (Type I nAChRs) mostly expressed presynaptically by glutamatergic afferents in the striatum, mecamylamine hydrochloride (MEC; 5 μm, Tocris) was used as a non-selective nAChRs antagonist that preferentially block Type III nAChRs [heterotrimeric α3β2β4, (Albuquerque et al., 1995, 2009)]. Atropine (Sigma, 10 μM) and scopolamine (Tocris, 10 μM) were used as non-selective mAChRs antagonists and VU0255035 (Tocris, 10 μM) as a selective M_1 mAChR antagonist. CNQX (10 μM, Tocris) and APV (10 μM, Tocris) to block respectively AMPA and NMDA glutamate receptors. We used tetrodotoxin (TTX, 1 μM, Sigma) in association with 4-aminopyridine (4-AP, 200 μM, Tocris) to isolate monosynaptic responses. Finally, to block gap junction (electrotonic) communication we used carbenoxolone (100 μM, Tocris).

Imaging

Mice were deeply anesthetized with an intraperitoneal injection of 80 mg/kg ketamine and 20 mg/kg xylazine. Brain tissue was fixed by transcardial perfusion of 10 mL of ice-cold artificial cerebrospinal fluid (adjusted to 7.2–7.4 pH), followed by perfusion of 90–100 mL of 4% paraformaldehyde, 15% picric acid diluted in phosphate buffer. Fixed brains were extracted and post-fixed overnight in the same solution. 50 μm sections were cut on a Vibratome 3000. Sections were mounted in Vectashield (Vector Labs, Burlingame, CA) and representative photomicrographs were taken using a confocal microscope (Fluoview FV1000, Olympus) using 10x or 40x objectives. Comparable photomicrographs were taken using the same laser settings.

After whole-cell recording, slices containing biocytin-filled neurons were transferred into 4% paraformaldehyde with 15% picric acid in 0.1 M PB for overnight fixation (4°C). After multiple washes in PBS, sections were incubated in PBS containing 0.05% Triton (3 h) followed by a blocking solution containing normal donkey serum (10%) and 0.05% Triton (2 h). Then, sections were incubated overnight with Streptavidin, Alexa Fluor 405 conjugate (Thermofisher, 1:1000) and an antibody against GFP (rabbit polyclonal anti-GFP, Invitrogen, 1:1000). Sections were then mounted in a fluorescence medium (ProLong Glass Antifade Mountant, Invitrogen) and representative photomicrographs were taken at 10x and 40x using a confocal microscope (Fluoview FV1000, Olympus). Images were processed using ImageJ software.

QUANTIFICATION AND STATISTICAL ANALYSIS

Patch-clamp recordings were analyzed using Signal, version 5 (Cambridge Electronic Design) and Axograph (version 1.3.4). Statistical analyses were performed using GraphPad Prism 9 software (San Diego, CA, USA). The statistical analyses were two-tailed statistical tests with alpha risk set at 0.05. All data were tested for normality using the Shapiro–Wilk test. For two-group comparisons we used two-tailed paired or unpaired t test depending on if the data resulted from the same cells or not, respectively. Further, one-way and two-way ANOVA followed by Tukey's post hoc test were used when comparing more than two datasets. In each experiment, results are presented as amplitude difference, percent change, p value(s), t value(s), statistical test used and cell number. Further animal number is indicated in each respective results section. Correlations between reduction of $GABA_{Afast}$ and $GABA_{Aslow}$ were done using a Pearson r correlation. Statistical significance is defined as *$p < 0.05$, **$p < 0.01$, ***$p < 0.001$, and ****$p < 0.0001$, if not noted otherwise.